VOLCΛNICΛ

A record of magmatic differentiation in plutonic xenoliths from Santorini (Greece)

Sean Whitley[α], ⬤ Ralf Halama[*α,β], ⬤ Ralf Gertisser[α], ⬤ Thor H. Hansteen[γ], ⬤ Matthias Frische[γ], and ⬤ Torsten Vennemann[δ]

[α] School of Geography, Geology and the Environment, Keele University, Keele, ST5 5BG, UK.

[β] Institute of Geosciences and Geography, Martin-Luther-Universität Halle-Wittenberg, Von-Seckendorff-Platz 3, 06120 Halle (Saale), Germany.

[γ] GEOMAR Helmholtz Centre for Ocean Research Kiel, Wischhofstrasse 1-3, D-24148 Kiel, Germany.

[δ] Faculty of Geosciences and Environment, Université de Lausanne, CH-1015 Lausanne, Switzerland.

ABSTRACT

Plutonic xenoliths from volcanic arcs provide unique insights into transcrustal magmatic systems in subduction zone settings. At Santorini volcano in the Central Aegean Volcanic Arc (Greece), plutonic xenoliths occur throughout a sequence of lavas and pyroclastic rocks erupted within the last ~360 ka. They are mineralogically variable, ranging from troctolites to olivine gabbros, gabbros, gabbronorites, and diorites. Thermobarometric calculations based on mineral and melt inclusion compositions indicate equilibration over a range of temperatures (1100 to 750 °C) at shallow to mid-crustal depths (P <400 MPa), but there is no evidence for crystallisation at lower crustal depths. Oxygen isotope data of mineral separates and calculated $\delta^{18}O_{melt}$ values are in line with extensive closed-system fractional crystallisation at magmatic temperatures, without a requirement for extensive assimilation of the subvolcanic continental basement. The xenolith minerals compositionally overlap with phenocrysts from the volcanic rocks, but they also contain evidence for the presence of highly evolved melt compositions in the form of melt inclusions with extremely silica-rich compositions (up to 82 wt.% SiO_2) and high enrichments of incompatible trace elements coupled with increasing negative Eu anomalies in clinopyroxenes. Since these characteristics correlate systematically with differentiation indices and rock type, they are interpreted to reflect melt evolution via fractional crystallisation as the dominant differentiation process with no significant role of reactive porous flow. These observations highlight that trapped melt fractions can influence mineral compositional variations in the plutonic xenoliths, and in turn the mineral compositions demonstrate a melt compositional variability not preserved in the volcanic rock record.

KEYWORDS: Santorini; Plutonic xenolith; Magmatic differentiation; Thermobarometry; Oxygen isotopes.

1 INTRODUCTION

Arc magmas typically show distinct geochemical and petrographic characteristics that represent a summation of the interplay of magma generation processes and magmatic differentiation, including magma mixing and crustal assimilation, during ascent. Much of the published work about the petrogenesis of arc magmas focuses on extrusive rocks and pays relatively little attention to plutonic xenoliths, although these are commonly found within the eruptive products of arc volcanoes [e.g. Arculus and Wills 1980; Beard 1986; Druitt et al. 1999; Turner et al. 2003; Martin et al. 2006; Holness et al. 2012; Chadwick et al. 2013; Stamper et al. 2014; Cooper et al. 2016; Klaver et al. 2017; Yanagida et al. 2018]. The term "plutonic xenoliths" refers to all coarse-grained igneous (plutonic) samples in lavas and volcaniclastic rocks that are derived from deeper parts of the magmatic plumbing system [Stamper et al. 2014]. The mineral compositions of plutonic xenoliths may correspond to those of antecrysts occurring in their host lavas or pyroclastics, and thus be genetically related to the eruption products. Eruptive products generally preserve and place constraints on pre-eruptive magmatic conditions and record geochemical and isotopic evidence of magma source composition and differentiation, whilst plutonic xenoliths can additionally provide direct insight into the early differentiation history and individual deep and shallow level magmatic processes that collectively determine the distinct geochemical and petrological trends found in the erupted rocks above subduction zones. Such plutonic xenolith studies have focused on reactive melt flow in the lower crust and its role in amphibole fractionation [Costa et al. 2002; Cooper et al. 2016; Klaver et al. 2017], oxygen isotope equilibration conditions [Tollan et al. 2012], polybaric differentiation of cumulus and phenocryst phases [Stamper et al. 2014; Klaver et al. 2017], magma differentiation trends [Druitt et al. 1999; Stamper et al. 2014; Cooper et al. 2019], and quantification of crustal assimilation [Brown et al. 2021].

This study focuses on the plutonic xenoliths found at Santorini volcano in the South Aegean Volcanic Arc (Greece) to elucidate the magmatic evolution of Santorini, complementing studies that have addressed this issue using constraints from extrusive igneous rocks. Many deposits of the explosive eruptions that occurred on Santorini since ~388 ka [Druitt et al. 1989; 1999; Vespa et al. 2006; Wulf et al. 2020; Satow et al. 2021] contain abundant plutonic xenoliths, ranging from microcumulate fragments at thin-section scale to fist-sized nodules. Previous studies of the plutonic xenoliths by Druitt et al. [1999] and Michaud et al. [2000] have estimated temperatures of cumulus phase formation and later re-equilibration temperatures, and highlighted the role of shallow crustal magma differentiation in andesite/dacite genesis, whereas Martin et al.

*✉ ralf.halama@geo.uni-halle.de

[2006] distinguished different types of mafic enclaves from the Kameni islands based on textural analyses (not considered in this study). This study uses compositional data of bulk rocks, minerals, including *in situ* laser ablation-inductively coupled plasma-mass spectrometry (LA-ICP-MS) trace element data, melt inclusions, and interstitial glasses coupled with oxygen isotope compositions of mineral separates to further constrain pressure and temperature conditions of plutonic xenolith formation and the compositional evolution of the magmatic system of Santorini.

2 GEOLOGICAL SETTING

Santorini is located in the South Aegean Volcanic Arc approximately 120 km north of Crete. The South Aegean Volcanic Arc is situated in the eastern Mediterranean Sea and is the result of the 50–60 mm y^{-1} [Jackson 1994] subduction of the African plate beneath the Aegean-Anatolian microplate, initiated 13 to 16 Ma ago [Le Pichon and Angelier 1979; Angelier et al. 1982; Mercier et al. 1989; Francalanci and Zellmer 2019; Papazachos 2019; Vougioukalakis et al. 2019]. Volcanism commenced in the late Pliocene [Pe-Piper et al. 1983].

Santorini consists of the three islands Thera, Therasia, and Aspronisi, which mark the outline of a flooded caldera. The post-caldera Palaea Kameni and Nea Kameni islands are situated within this caldera (Figure 1). Pre-volcanic Triassic to Palaeocene basement crops out at Athinios and Mount Profitis Ilias on Thera, comprising blueschist to amphibolite facies metapelites and crystalline limestones [Davis and Bastas 1978; Skarpelis and Liati 1990; Kilias et al. 1998; Druitt et al. 1999]. Volcanic activity is strongly influenced by two NE–SW trending tectonic lineaments, the Kameni and Kolumbo lines [Druitt et al. 1999; Klaver et al. 2016; Nomikou et al. 2019], and the earliest volcanic activity started about 650 ka ago at the Akrotiri peninsula, producing amphibole-bearing silicic tuffs and lava flows [Davis et al. 1998; Dietrich et al. 1998; Druitt et al. 1999; Mortazavi and Sparks 2004]. This was followed by eruption of magmas bearing dominantly anhydrous phases, starting with the Peristeria volcano (530–430 ka) (Figure 1). This modern (post-530 ka) magmatic differentiation dominated by an anhydrous phase assemblage [Nicholls 1971b; Huijsmans et al. 1988; Druitt et al. 1999; Eiler et al. 2000; Druitt et al. 2019] contrasts with many arc volcanoes that show phenocryst or geochemical evidence for pervasive amphibole fractionation during their petrogenesis [e.g. Davidson et al. 2007]. Twelve major Plinian-style eruptions have occurred since ~360 ka, forming the Thera Pyroclastic Formation [Druitt et al. 1989; 1999; Wulf et al. 2020]. Two cycles of mafic to silicic magma evolution have been identified in the post 360 ka deposits, each ending with large magnitude caldera forming eruptions, including, possibly, the 185.7 ka Lower Pumice 1 and the 176.7 ka Lower Pumice 2 eruptions at the end of the first cycle, as well as the 22 ka Cape Riva and the 3.6 ka Minoan (Late Bronze Age) eruptions at the end of the second cycle [e.g. Druitt et al. 1999; Gertisser et al. 2009; Druitt 2014; Simmons et al. 2017; Wulf et al. 2020]. Another caldera may have formed incrementally and was established at around 67 ka [Druitt et al. 1999]. Interplinian activity included Strombolian and sub-Plinian explosive activity, lava flows and extrusive edifice construction

[e.g. Huijsmans 1985; Barton and Huijsmans 1986; Edwards 1994; Druitt et al. 1999; Vespa et al. 2006; Vaggelli et al. 2009; Fabbro et al. 2013; Karátson et al. 2018; Pank et al. 2022]. Integration of on-land stratigraphy and sea-level record combined with numerical modelling suggests that the timing of eruptions on Santorini is modulated by variations in sea level [Satow et al. 2021].

Recent petrological work at Santorini has focused on constraining pre-eruptive magmatic conditions derived from experimental petrology [Cottrell et al. 1999; Cadoux et al. 2014; Andújar et al. 2015; 2016], volatile solubility [Druitt et al. 2016], and diffusion modelling [Druitt et al. 2012; Fabbro et al. 2018; Flaherty et al. 2022] of the eruptive products, which forms the framework for this study. Compositionally, the eruptive products of Santorini range from low- to high-K basalt to rhyodacite, transitional tholeiitic to calc-alkaline [Huijsmans et al. 1988; Druitt et al. 1999; Bailey et al. 2009; Fabbro et al. 2018]. Olivine-hosted melt inclusions preserve evidence for melt generation in a depleted peridotitic mantle modified by slab-derived agents with a chemical composition indicative of sediment melts [Flaherty et al. 2022]. Sr-Nd-Pb isotopic and trace element studies indicate varying (~10 %) contamination of Santorini magma with upper Aegean continental crust during fractional crystallisation, with at least some of the contamination having occurred in upper crustal reservoirs [Druitt et al. 1999, and references therein]. Phase equilibria [Cadoux et al. 2014; Andújar et al. 2015; 2016] and fluid saturation studies [Druitt et al. 2016] have shown differentiation of parental basalts (50 wt% SiO_2, 7 wt% MgO, 1–4 wt% H_2O) to andesite at about 400 MPa (~16 km depth), and to silicic compositions at around 200–400 MPa (~8–16 km depth), before storage and eruption from reservoirs at shallow depths of a few kilometres (100–160 MPa; ~4–6 km depth). A variety of xenoliths has long been identified throughout the Santorini volcanic succession, including plutonic xenoliths (the focus of this study) but also basement fragments and calc-silicate assemblages metamorphosed by their host magma [e.g. Fouqué 1879; Lacroix 1900; Nicholls 1971a; Barton and Huijsmans 1986; Druitt et al. 1999; Druitt 2014]. Amphibole-bearing mafic inclusions from the early Akrotiri centre have been covered by Mortazavi and Sparks [2004], highlighting differentiation from a wet (>4 % H_2O) basaltic magma involving amphibole fractionation during the petrogenesis of early Santorini magmas.

3 METHODS

Analytical methods are presented in Appendix A.1 (Supplementary Material 1). Electron microprobe measurements were carried to determine major element and volatile (Cl, S) concentrations in minerals and glasses (see Table S1 in Supplementary Material 2 for standard reference material data). Laser ablation-inductively coupled plasma-mass spectrometry was used to measure trace element contents in minerals and glasses (see Table S2 in Supplementary Material 2 for standard reference material data). Whole-rock powders were analysed by X-ray fluorescence for major and selected trace elements of the bulk xenoliths. Mineral oxygen isotope compositions were analysed for olivine, pyroxene and plagioclase separates. Appendix A.2 (Supplementary Material 1) outlines the major ele-
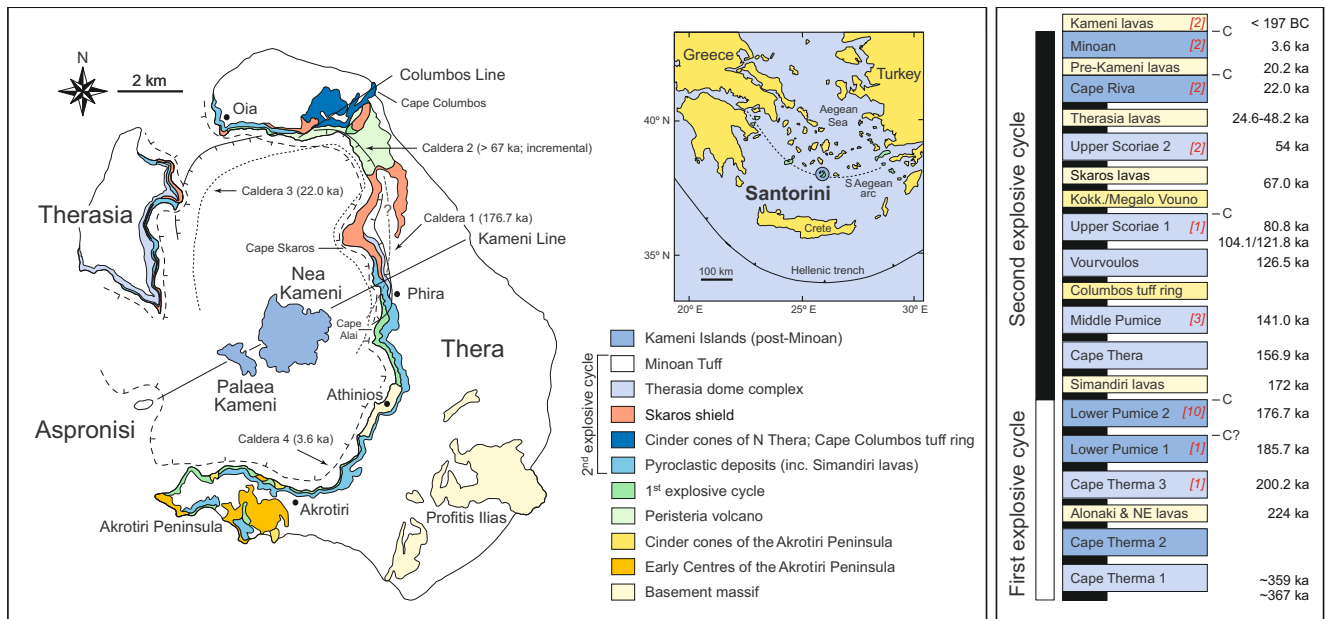
Figure 1: Location map, geological map and stratigraphy for the past ~360 ky of volcanic activity of Santorini [after Druitt et al. 1999], updated with ages from Druitt et al. [1999], Fabbro et al. [2013], Karátson et al. [2018], Vakhrameeva et al. [2018], and Wulf et al. [2020]. Eruptions marked in dark blue in the stratigraphic column are dominantly silicic eruptions, whereas light blue denotes eruptions intermediate in composition. Black bars are inter-Plinian intervals of minor explosive eruptions; light and dark yellow bars are prominent inter-Plinian lava successions and monogenetic cones/tuff rings, respectively [after Vespa et al. 2006; Druitt et al. 2016; Wulf et al. 2020; Satow et al. 2021]. C = caldera collapse. Red numbers in brackets denote the number of xenoliths sampled from the different units; see Table 1 for details of eruptions sampled.

Table 1: Samples analysed in this study

Sample	Eruption	Rock type	Petrography	Modal composition	Mineral and glass chemistry	Whole-rock composition	Oxygen isotope composition
SAN 11-2-1-6	Nea Kameni	Gabbro	×		×		
SAN 5-2-1u	Nea Kameni	Troctolite	×	×	×	×	
SAN 4-4c	Minoan	Gabbro	×	×	×	×	
SAN 9-3-2	Minoan	Gabbronorite	×		×	×	
SAN 5-3-4 (3)	Cape Riva	Diorite	×		×		
SAN 12-1-5	Cape Riva	Gabbronorite	×		×	×	×
SAN 12-1-8-2	Upper Scoria 2	Diorite	×		×	×	
SAN 14-1-1-3	Upper Scoria 2	Gabbronorite	×		×		×
SAN 12-2-2	Upper Scoria 1	Gabbronorite	×	×	×	×	
SAN 6-5-2-1	Middle Pumice	Olivine gabbro	×	×	×	×	
SAN 6-5-3	Middle Pumice	Diorite	×	×	×	×	
SAN 9-2-2	Middle Pumice	Gabbro	×	×	×	×	×
24D	Lower Pumice 2	Olivine gabbro	×	×	×	×	
27D	Lower Pumice 2	Olivine gabbro	×				
28D	Lower Pumice 2	Diorite	×	×	×	×	
SAN 9-1-1-3	Lower Pumice 2	Gabbronorite	×		×		
SAN 9-1-3	Lower Pumice 2	Gabbro	×			×	
SAN 9-1-4	Lower Pumice 2	Gabbro	×			×	
SAN 9-1-5	Lower Pumice 2	Gabbro	×	×			
SAN 9-1-8-1	Lower Pumice 2	Olivine gabbro	×				×
SAN 9-1-8-2	Lower Pumice 2	Olivine gabbro	×				×
SAN 9-1-8-3	Lower Pumice 2	Gabbro	×	×	×		
SAN 6-4-2	Lower Pumice 1	Gabbro	×		×	×	
SAN 6-3-1	Cape Therma	Gabbro	×		×		×

ment data corrections for melt inclusion post-entrapment crystallisation (PEC). A description and justification of the geothermobarometers used is presented in Appendix A.3 (Supplementary Material 1). Appendix A.4 (Supplementary Material 1) provides details about the calculation of the mineral-melt trace element partition coefficients used to derive equilibrium melt compositions from mineral trace element data.

4   RESULTS

4.1   Xenolith petrography

Xenoliths are abundant in many of the eruptive units (Figure 2). Twenty-four plutonic xenoliths have been chosen for detailed study (Table 1), covering the range of lithologies observed, prioritising the least altered samples based on hand specimen and thin-section inspection. Analysis of 144 thin-sections from the full stratigraphy shows five dominant lithologies based on the classification of Streckeisen [1974]: troctolite, olivine gabbro, gabbro, gabbronorite, and diorite (Figures 3 and 4). Troctolites typically occur as glomerocrysts. Plutonic xenoliths are classified as diorite instead of gabbro or gabbronorite when the compositions of the feldspar cores are dominantly less than An_{50}. Santorini magmas are characteristically amphibole free post 530 ka [Druitt et al. 1999], therefore the name diorite is purely based on feldspar composition [Streckeisen 1974], and does not imply a dominance of amphibole over clinopyroxene as the main ferromagnesian mineral phase. Since there is no systematic relationship between xenolith type and stratigraphy, and as the xenoliths may not necessarily be cogenetic to the eruption they are from (see Section 5), the rock types will be discussed by lithology in the following section.

4.2   Troctolite glomerocrysts

Centimetre-sized angular troctolitic glomerocrysts are found in some of the lavas sampled on Nea Kameni (Figure 4A). They comprise small (~300 µm) rounded olivine grains (<25 vol%, Figure 4A) enclosed in large millimetre-sized weakly zoned plagioclase crystals. Plagioclase is often surrounded by a rim of clinopyroxenes and/or glass lacking the devitrified microlitic texture of the lavas at the lava contact, and this glass infiltrates the fragments. Strained plagioclase twins are present. These samples are similar to the gabbroic and troctolitic cumulate glomerocrysts previously described by Martin et al. [2006].

4.3   Olivine Gabbro

Rare olivine-gabbros occur in the deposits of the Lower Pumice 2 and Middle Pumice eruptions. They are up to a centimetre in size, coarse-grained and rounded. They comprise an assemblage of up to 2 mm-sized crystals of olivine (5–10 vol%), clinopyroxene and plagioclase, with abundant interstitial glass, plagioclase and clinopyroxene microlites, and trace amounts of interstitial amphibole (Figure 4B). Infrequent micrometre-sized magnetite is restricted to clinopyroxene and olivine grain-glass boundaries, excluding sample 27D (Lower Pumice 2) in which they occur up to 500 µm in size, spread throughout the sample. Crystal forms are generally euhedral
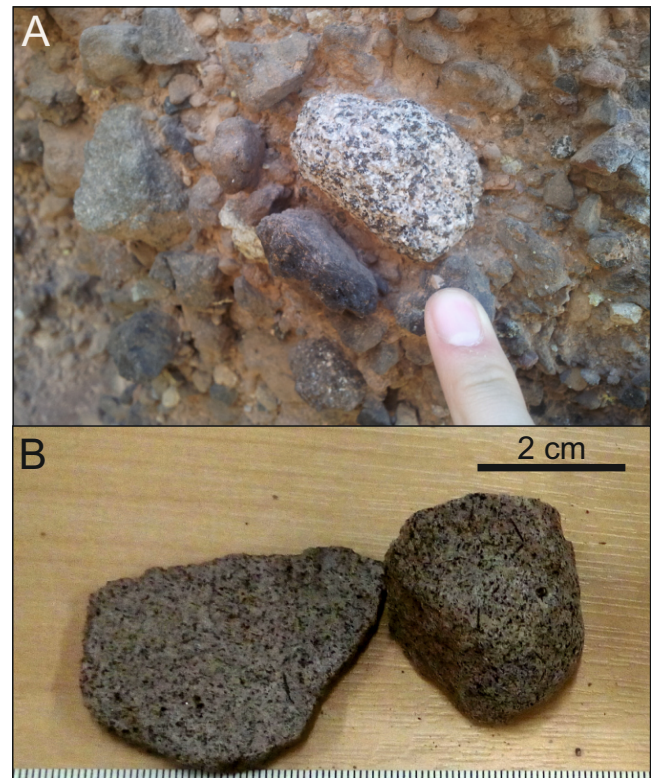

Figure 2: [A] Gabbro xenolith in the deposits of the Cape Therma 3 eruption. [B] Hand specimen photograph of diorite xenolith SAN 12-1-8-2 from the Upper Scoria 2 eruption.

to subhedral. Plagioclase texturally appears to be the first crystallising phase, followed by clinopyroxene and olivine. Plagioclase has different textural features: unzoned crystals, very weakly oscillatory zoned crystals and crystals with strongly resorbed cores (Figure 4C) containing glass, clinopyroxene, and magnetite microlites. Rare plagioclase exhibiting these textures has been described in the pyroclastic deposits of the Lower Pumice 2 eruption as antecrysts from cumulates [Gertisser et al. 2009]. In contrast to the more common gabbroic lithologies, olivine gabbros are relatively well preserved. Olivine exhibits partial iddingsitisation on the rims and along fractures. Melt inclusions are exceptionally abundant within clinopyroxene and plagioclase in some samples. Depending on the sample and host phase, these melt inclusions often contain numerous daughter crystals and/or evidence of alteration, indicating significant post-entrapment modification (Appendix A.1, Supplementary Material 1). Olivine-hosted melt inclusions are rarer and show less evidence of alteration.

4.4   Gabbro

The gabbro xenoliths range in size from centimetre-sized pieces to fist-sized blocks, in rounded to sub-angular pieces. They comprise dominantly coarse-grained (up to 2 mm) clinopyroxene and plagioclase with minor interstitial glass, Fe-Ti oxides, quartz, orthoclase, and apatite (Figure 4D-F). The clinopyroxenes are commonly unzoned, however some samples show clinopyroxene with irregular zoning and a sharp rim. Plagioclase is strongly zoned, with a distinct contact be-
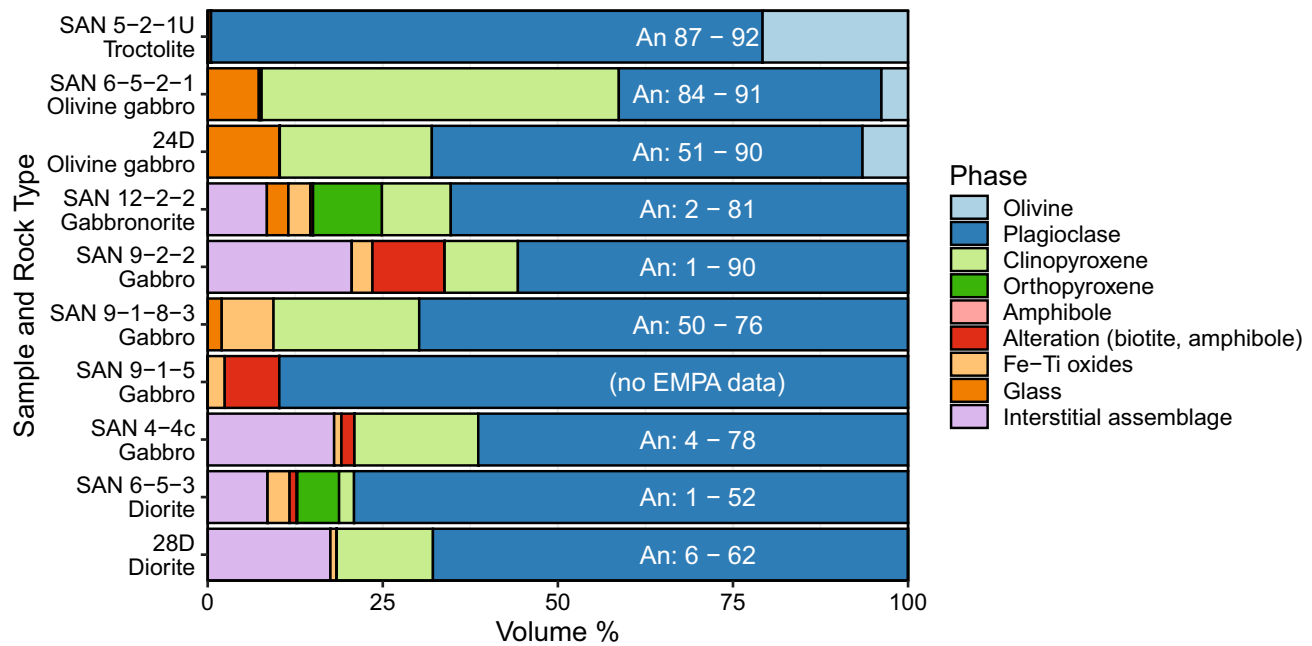
Figure 3: Modal mineralogy of representative xenoliths. Alteration products are generally biotite/amphibole replacing clinopyroxene. Texturally, the majority of hydrous phases in the samples are a result of secondary alteration and not part of the primary igneous mineral assemblage. Anorthite numbers (X_{An}) given for plagioclase include rim compositions and interstitial crystals. Glass in the olivine gabbros contains microlites of plagioclase, clinopyroxene, olivine and amphibole. The interstitial assemblage in the gabbros and gabbronorites is generally quartz with minor orthoclase and glass.

tween the core and a more gradual mantle to rim profile. The cores can be patchy, and on rare occasions more sodic than the mantle and rims. Clinopyroxene is commonly rimmed or fully replaced by actinolite and biotite, with minor titanite, ilmenite, and rutile. Fe-Ti oxides commonly exhibit exsolution lamellae of ilmenite in titanomagnetite.

4.5 Gabbronorite

Gabbronorite xenoliths are rounded to sub-angular and up to 5 cm in size. They comprise clinopyroxene, orthopyroxene, strongly zoned plagioclase, Fe-Ti oxides, trace amphibole, apatite, and interstitial glass in fine-grained (<0.5 mm crystal size) and medium-grained (<2 mm crystal size) varieties (Figure 4G). Clinopyroxene and orthopyroxene are commonly unzoned and have a distinct rim at the contact with plagioclase, orthoclase, and (rare) glass of the interstitial assemblage. In finer-grained xenoliths the pyroxenes show acicular needle-like habits, changing from clinopyroxene to orthopyroxene along their length, but lacking clear exsolution lamellae. Rare olivine (<1 vol%) with two-pyroxene-bearing reaction rims is found in two samples. Plagioclase often has a distinct weakly zoned core and more pronounced zonation towards the rims. Fe-Ti oxides often show exsolution lamellae, and partial transformation of pyroxene to amphibole and biotite is common in both the fine- and medium-grained varieties.

4.6 Diorite

Diorite xenoliths comprise clinopyroxene, strongly zoned plagioclase, orthopyroxene in some samples, Fe-Ti oxides, trace

amphibole, and interstitial glass (Figure 4H). They are texturally similar to some of the more evolved gabbro and gabbronorite samples, additionally containing an interstitial assemblage of albite-rich plagioclase, orthoclase, and rare interstitial glass.

4.7 Mineral compositions

The full mineral datasets are available in Supplementary Material 2 (Tables S3–S7).

4.7.1 *Olivine*

Troctolitic glomerocryst olivine in sample SAN 5-2-1u is the most primitive and least altered in our study, with Fo_{77-84} and CaO = 0.14-0.21 wt% (Figure 5A, Supplementary Material 2 Table S3). These are more evolved than compositions reported by Martin et al. [2006] for their Nea Kameni cumulate fragments (Fo_{85-93}). In the olivine gabbros, each sample contains compositionally homogeneous olivine, with <2 mol% Fo variation per sample (overall range Fo_{74-78} and CaO = 0.16–0.23 wt%), except for small interstitial olivines in the glass (Fo_{65-75}, CaO = 0.19–0.43 wt%). Gabbronorite olivine is more evolved (Fo_{47-69}, CaO = 0.01–0.23 wt%) and always surrounded by a rim of clinopyroxene or orthopyroxene. The samples with Fo < 60 are from sample SAN 12-1-5, which only contains this olivine composition. CaO is weakly correlated with Fo content. Transition metals are the only dominant detectable trace elements present (Co 202–206 ppm, Zn 137–175 ppm, Ni 442–608 ppm, Cu 2.6–4.1 ppm). REE concentrations are very low ($\sum$REE 0.07 ppm) with a weak
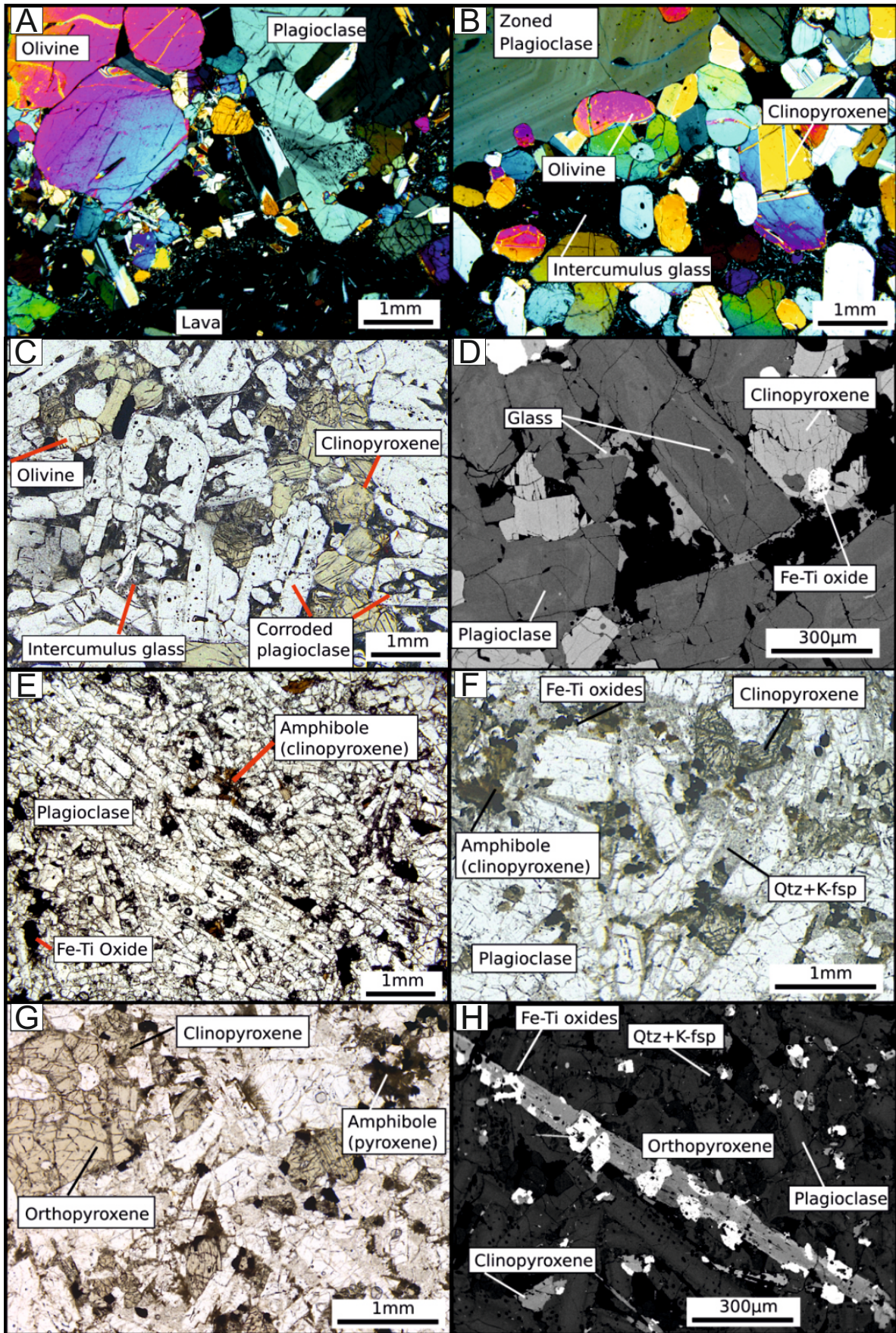
Figure 4: (Caption next page.)

Figure 4: (Previous page.) Petrography of the xenoliths. [A] Troctolite with clinopyroxene-rich rim at the lava contact (sample SAN 5-2-1U, Nea Kameni). [B] Olivine gabbro with interstitial glass (sample 24D, Lower Pumice 2). [C] Corroded plagioclase with glass-filled cores in olivine gabbro (sample 27D, Lower Pumice 2). [D] Mafic glass-bearing gabbro with patchy zoned plagioclase (sample SAN 9-1-8-3, Lower Pumice 2). [E] Gabbro showing layering of plagioclase (sample SAN 9-1-5, Lower Pumice 2). [F] Intermediate holocrystalline gabbro with secondary amphibole replacing clinopyroxene (sample SAN 9-2-2, Middle Pumice). [G] Coarse-grained gabbronorite (sample SAN 14-1-1-3, Upper Scoriae 2). [H] Fine-grained diorite with acicular pyroxene crystals (sample SAN 6-5-3, Middle Pumice). Many gabbronorite samples are texturally indistinguishable from this sample. [A], [B] and [C], [E], [F], [G] are thin-section microphotographs obtained with crossed nicols and in plane polarised light, respectively; [D] and [H] are back-scattered electron images.

relative enrichment in HREE, and LREE typically below the detection limit.

4.7.2 Clinopyroxene

Crystal core Mg# generally decreases from the olivine gabbros (Mg# 76–86) through gabbros (Mg# 60–82), diorites (Mg# 68–71) to gabbronorite (Mg# 55–80) (Figure 5B, C; Supplementary Material 2 Table S4). Clinopyroxene in the rim around the troctolitic glomerocrysts and as small crystals within the glomerocrysts has Mg# 58–72, much lower than the olivine (Fo$_{79–84}$) and overlapping the Mg# of the clinopyroxenes in the host lava within this sample (Mg# 70–82). Clinopyroxene crystals across the xenoliths are commonly unzoned, with some samples having a fine 5–15 μm rim with a lower Mg# in contact with the interstitial assemblage. Olivine gabbro clinopyroxenes have little compositional variation within samples (<4 mol% Mg#) but exhibit the distinct sharply bound Fe-rich rim (Mg# 64–73) at the contact with interstitial glass, and Fe-rich microlites within the glass (Mg# 59–65). Clinopyroxene within the gabbros, gabbronorites and diorites shows a wider compositional range within samples, and the crystals within some samples show patchy zonation unrelated to growth zones. Al$_2$O$_3$ concentrations in clinopyroxene are higher and fall into a more restricted range in the olivine gabbros (core 2.7–3.8 wt%, rim and interstitial: 5.1–7.8 wt%) compared to the gabbros and gabbronorites (<3.8 wt%, with the majority below 2.5 wt%). Clinopyroxene compositions generally overlap compositions of phenocrysts from the pyroclastic deposits, but some gabbro, diorite, and gabbronorite samples distinctly differ, with low Al, Ti, and Mn concentrations in clinopyroxene (Figure 5B, C). These compositions do not match any of the experimentally produced clinopyroxenes from Cadoux et al. [2014] or Andújar et al. [2015, 2016] on Santorini liquid compositions, but overlap the compositions of many hydrothermally altered clinopyroxenes in the literature [Manning and Bird 1986; Rose and Bird 1994; Good et al. 1997; Martinez-Serrano 2002; Marks et al. 2010]. In contrast to the low Ti-Al cluster, clinopyroxenes from diorite samples SAN 6-5-3 and SAN 12-1-8-2 have elevated TiO$_2$ and Al^{IV} relative to the volcanic field.

REE profiles of clinopyroxenes are generally concave, with moderate MREE and HREE enrichment relative to the LREE ((La/Sm)$_N$ = 0.21–0.75, (Gd/Lu)$_N$ = 0.94–2.17, Figure 6A). Overall REE enrichment generally correlates with the xenolith type, with olivine gabbro clinopyroxenes showing up to 10× enrichment relative to chondrite (normalisation values from Palme and O'Neill [2014]) and gabbronorite clinopy-

roxenes showing up to 500× enrichment. Five samples do not follow these profiles and have flatter or negative slopes with high La/Yb = 0.99–3.45 (Figure 6B). Some of these samples additionally fall into the low Ti-Al major element group. These profiles have similar characteristics (negative slope and slight relative LREE enrichment) to the few amphibole analyses made. There is no clear correlation between REE profile slope and clinopyroxene major element composition (Ti, Al^{IV}, Mg#, Na), indicating that major element crystal composition is not controlling these anomalous slopes (Figure 6C). Overall, clinopyroxenes from the plutonic xenoliths have negative Eu anomalies that correlate with differentiation indices such as decreasing Mg# and increasing La (Figure 6D), but do not correlate with some other incompatible trace element concentrations (e.g. Zr). Similarly to the REE, normalized trace element profiles show features that change systematically with rock type and increase/decrease with the degree of differentiation of each xenolith.

4.7.3 Orthopyroxene

Mg# ranges between 46–76, and crystals commonly have a rim of Mg# = 46–55 (Table S5, Supplementary Material 2). Al$_2$O$_3$ concentrations are <3.5 wt%, with the bulk of orthopyroxenes containing <2 wt%, increasing with Mg#. Excluding three outliers reaching 9 mol%, Wo content ranges from 1.3 to 4.6 mol%. As with the clinopyroxenes, most samples fall within the compositional range of orthopyroxene from eruptive units found in the literature. However, orthopyroxenes from two gabbronorite samples plot distinctly away, having high Ti-low Mg# (SAN 12-1-5) and low Ti-high Mg# populations (SAN 9-1-1-3) (Figure 5D). REE concentrations are low (∑REE = 4.94–28.85 ppm) and profiles show an enrichment of MREE and HREE relative to LREE ((La/Yb)$_N$ = 0.003–0.259, Figure 6E) with varying negative Eu anomalies (0.08–0.87) that have no systematic correlation with Mg#.

4.7.4 Feldspar

Feldspar, dominantly zoned plagioclase, is present in every sample (Figure 5E, Supplementary Material 2 Table S6). Plagioclase from the troctolites (An$_{93–86}$) and olivine gabbros (An$_{91–84}$) are weakly oscillatory zoned crystals with <5 % An variation within samples regardless of crystal texture (sieve or homogeneous). These are within the range of An$_{95–85}$ identified in the Nea Kameni cumulate xenoliths of Martin et al. [2006]. Plagioclase has a higher An content than the Fo content in coexisting olivine (Fo$_{78–74}$), as is commonly observed in volcanic arcs [e.g. Arculus and Wills 1980; Sisson and Grove
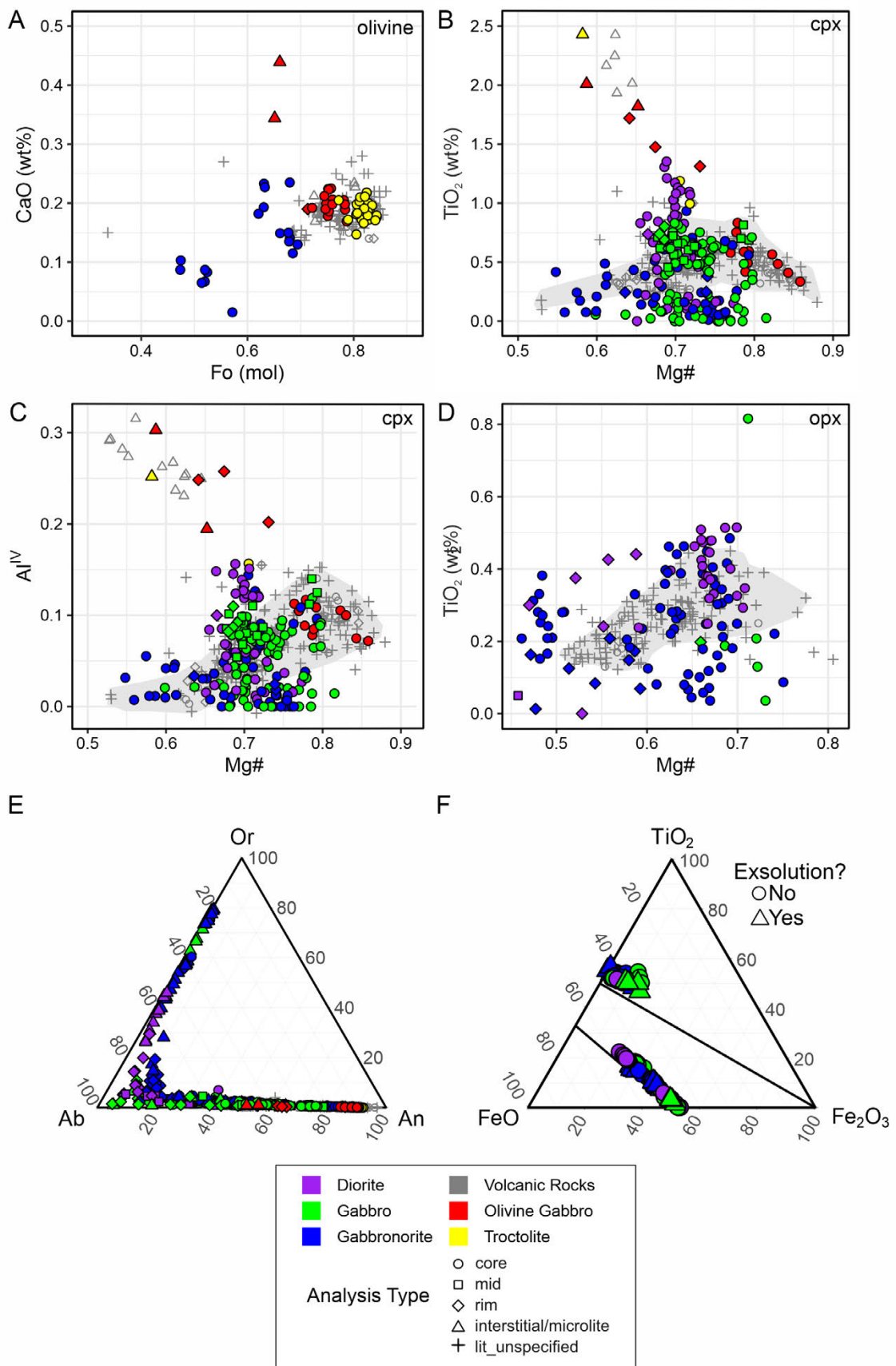
Figure 5: (Caption next page.)

Figure 5: (Previous page.) Major element mineral compositions of the xenoliths. [A] Olivine. Literature data of olivines from volcanic rocks (light grey symbols) are from Druitt [1983], Cabato [2007], Gertisser et al. [2009], Druitt et al. [2016]. [B] and [C] Clinopyroxene. Grey fields show the general trend of published clinopyroxene compositions from volcanic rocks. Xenolith clinopyroxenes broadly follow the volcanic trend. Notably a low Ti-Al cluster forms at intermediate Mg# compositions. Diorite samples show a distinct trend with increasing TiO_2-Al^{IV} at near constant Mg#. Interstitial and microlite samples with increasing TiO_2-Al^{IV} at low Mg# can be attributed to rapid element uptake during rapid cooling [Mollo et al. 2010]. Literature data from Druitt [1983], Huijsmans [1985], Barton and Huijsmans [1986], Cottrell et al. [1999], Cabato [2007], Gertisser et al. [2009], Vaggelli et al. [2009], Panienka [2012], Cadoux et al. [2014], Andújar et al. [2015], and Druitt et al. [2016]. [D] Orthopyroxene. TiO_2 vs Mg# showing a wide spread of data compared to orthopyroxenes from volcanic rocks. Literature data (light grey) from Druitt [1983], Huijsmans [1985], Cabato [2007], Gertisser et al. [2009], Panienka [2012], and Druitt et al. [2016]. [E] Feldspar. Compositions plotted in the ternary An-Ab-Or diagram. Literature data of feldspars from volcanic rocks are from Druitt [1983], Cabato [2007], Panienka [2012], Druitt et al. [2012], and Druitt et al. [2016]. [F] Fe-Ti oxides.

1993; Tollan et al. 2012]. Although the interiors of the plagioclase crystals in the olivine gabbro are essentially unzoned, they possess a very distinct sharp rim of An_{65-62} in contact with the interstitial glass. Plagioclase zoning within the gabbros, diorites, and gabbronorites is significantly more variable and can be weakly oscillatory, distinctly patchy, or radially diffuse across the crystal. The crystal cores commonly comprise a high An zone (up to An_{90}) with a resorption texture, and strong normal zoning to $An_1Ab_{99}Or_6$ at the rims in contact with the interstitial assemblage. FeO is positively correlated to An content. Some gabbros and gabbronorites have plagioclase cores with lower An content than the normal zoned mantle to rim zones. K-feldspar occurs as rim to plagioclase with up to 58 mol% orthoclase and as an interstitial phase with up to 79 mol% orthoclase. Incompatible trace elements (Ba, Sr, La) are inversely correlated with An content and relatively enriched in crystal rims compared to cores (Figure 6F). REE concentrations are low ($\sum$REE = 0.42–31.35 ppm) and show a LREE enrichment relative to MREE and HREE ($(La/Yb)_N$ = 5–114) with a strong positive Eu anomaly inversely correlated to An mole fraction.

4.7.5 *Amphibole and biotite*

Amphiboles (Table S7, Supplementary Material 2) are classified based on the scheme of Hawthorne et al. [2012] using the classification spreadsheet of Locock [2014]. Amphibole microlites within the olivine gabbro interstitial glass are magnesioferri-hornblende. Primary interstitial amphiboles within the gabbronorite are predominantly magnesio-ferri-hornblende. Actinolite ($Al^{IV} < 0.5$) is the dominant amphibole type, found as a secondary replacement phase. Xenolithic amphibole, whether primary or secondary, typically has lower Al^{IV} (< 1.4) than the microlite amphibole found in the Lower Pumice 2 [Gertisser et al. 2009] or the Akrotiri phenocrysts [Mortazavi and Sparks 2004], highlighting a clear compositional difference. REE slopes for a small number of amphibole analyses ($n = 5$) are generally negative, with $(La/Yb)_N$ between 0.91 to 1.89. Biotite is replacing clinopyroxene, with Mg# between 0.49 and 0.77, and Al_2O_3 between 9.34 and 14.18 wt%.

4.7.6 *Fe-Ti oxides*

Both magnetite and ilmenite are present across the xenoliths (Table S7, Supplementary Material 2), but not always coexisting. Evidence of exsolution of ilmenite lamellae in magnetite is

common and additionally secondary alteration in some samples is shown by red oxidised rims. Compositions lie on the ulvöspinel-magnetite exchange vector (Figure 5F). TiO_2 in magnetite ranges from 0.03 to 17 wt% and Cr_2O_3 is predominantly less than 0.2 wt%, with one analysis reaching 1.4 wt%.

4.8 Whole-rock, melt inclusion, and interstitial glass compositions

Plutonic xenolith whole-rock compositions (calculated from point counting combined with averaged mineral and glass chemistry [Whitley et al. 2020] and measured; Table 2) broadly follow the liquid line of descent for Santorini, with a few that fall off the trend for various elements (Figure 7). SiO_2 concentrations range from 46 to 65 wt%. The olivine gabbros and intermediate glass-bearing gabbros are mafic (SiO_2 46–49 wt%) whilst the gabbros and gabbronorites are dominantly intermediate, both spanning a range from 52 to 65 wt% SiO_2. The high TiO_2 in the most SiO_2-poor xenolith (SAN 9-1-8-3) is due to a large modal proportion (7.4 vol%) of titanomagnetite. A low K_2O group diverging from the general trend is formed from samples almost entirely composed of clinopyroxene and plagioclase, similar to three gabbroic xenoliths analysed in Druitt et al. [1999]. Six olivine gabbro and gabbro xenoliths have systematically 3 to 5 wt% lower FeO concentrations than the liquid line of descent, but gabbronorites and diorites are on the trend. Four gabbro xenoliths have Na_2O concentrations up to 3 wt% higher than equivalent SiO_2 lava whole rocks, lying at an extension of an inflection in Na_2O in the literature data and xenolith glass analyses (Figure 7).

Melt inclusion and interstitial glass analyses from the xenoliths (44 to 82 wt% SiO_2) cover almost the entire compositional range of published whole rock, melt inclusion, and glass analyses for the Santorini rocks (40–79 wt% SiO_2), with only melt inclusions from gabbroic inclusions at Nea Kameni [Michaud et al. 2000] extending to lower SiO_2 (Table S8). Xenolith glass compositions extend to higher SiO_2 concentrations however, reaching 82 wt% SiO_2 in the interstitial glass and in melt inclusions in the gabbronorites (Table S8, Supplementary Material 2). Some deviations from the eruptive liquid line of descent are observed.

Concentrations of trace elements including the REEs in melt inclusions and interstitial glass from the olivine gabbros and a glass-rich gabbro (SAN 9-1-8-3, LP2 eruption) fall within
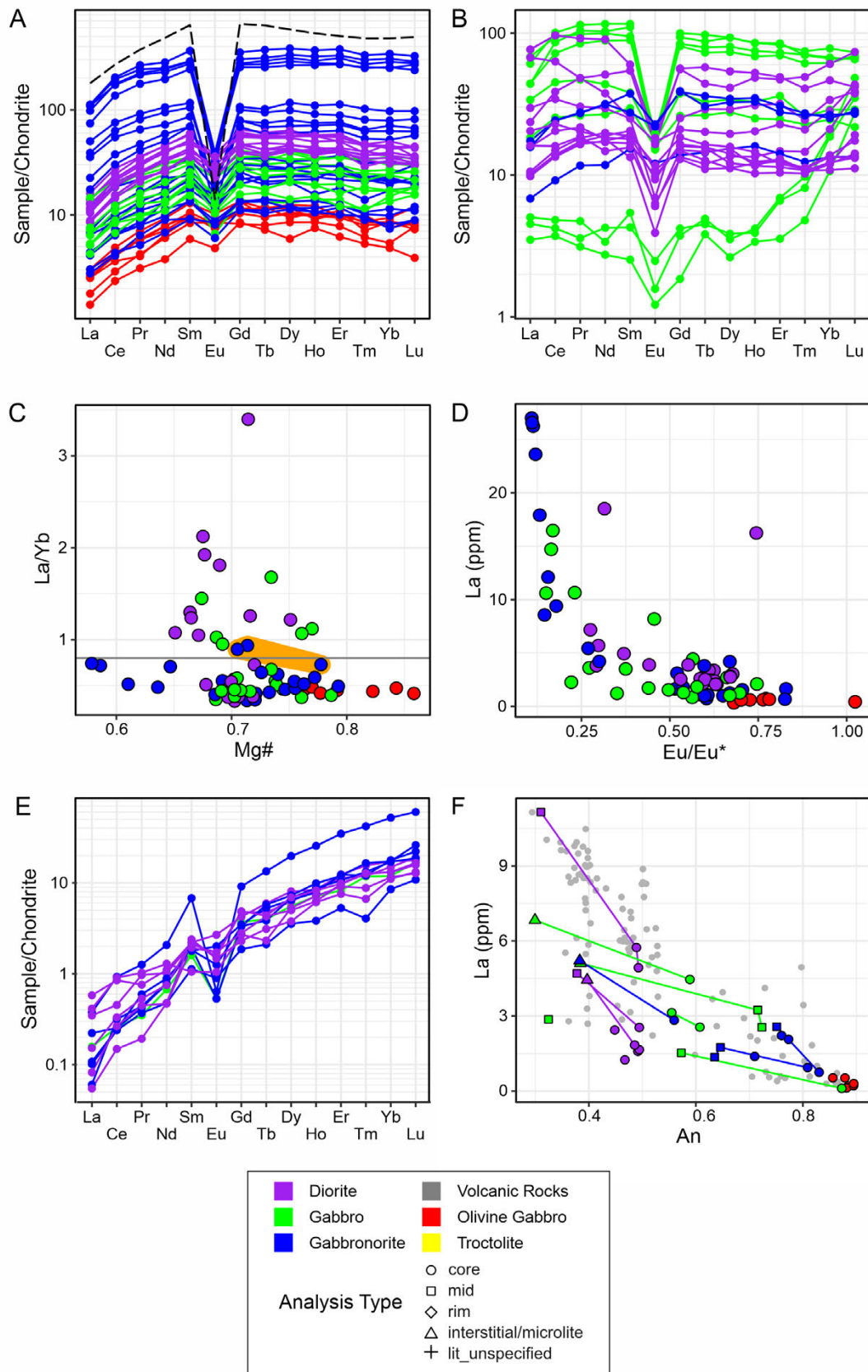
Figure 6: (Caption next page.)

Figure 6: (Previous page.) Trace element mineral compositions. All normalisation values from Palme and O'Neill [2014]. [A]–[D]: Clinopyroxene. [A] Chondrite-normalized rare earth element (REE) profiles. The black dashed line represents the composition of a clinopyroxene crystallising from the final stage of closed system crystallisation of a mafic cumulate (see discussion). [B] Chondrite-normalized REE profiles for samples with anomalous profiles. These clinopyroxenes have a slight enrichment in LREE and MREE compared to HREE. [C] La/Yb vs Mg# showing the normal clinopyroxene slopes (below the line) compared to anomalous slopes. Sample SAN 9-3-2 is highlighted in orange, representing a non-cogenetic Minoan eruption xenolith (see Discussion and Druitt [2014]). [D] La vs Eu anomaly showing a good negative correlation, excluding two outlier points, indicating a strong role in fractional crystallisation influencing clinopyroxene REE enrichment (see Section 5). Eu/Eu^* is calculated as $Eu/Eu^* = Eu_N/(Sm_N * Gd_N)^{0.5}$ [Taylor and McLennan 1985]. [E] Orthopyroxene. Chondrite-normalised REE profiles. [F] Feldspar. La (ppm) vs An (mol) showing core to rim incompatible trace element enrichment. Literature data for feldspar from pumice in grey from Santo [2005], Druitt et al. [2012], and Fabbro et al. [2018].

almost the entire range of literature whole-rock analyses (Figure 8). Melt inclusions have distinctly lower REE concentrations than interstitial glasses. Interstitial glass and melt inclusions in the gabbronorites were too small for reliable analysis, but it is expected these would have strong enrichments in trace elements, based on their high SiO_2 contents and high trace element concentrations in host minerals (e.g. clinopyroxene) relative to other lithologies. REE profile slopes ($(La/Lu)_N$ = 0.99–5.18) become more negative due to a relative LREE enrichment over HREE in more felsic glass compositions, a feature also noted by Elburg et al. [2014]. Trace element data include profiles that are more primitive than the bulk of the volcanic rock dataset (Figure 8).

4.9 Oxygen isotope compositions

Oxygen isotope analyses were made on the least altered samples from the most abundant rock types with sufficient sample material (olivine gabbro, gabbro, and gabbronorite) (Figure 9, Table 3). In olivine gabbros, plagioclase (n = 3) has $\delta^{18}O$ of 6.3 to 6.4 ‰, clinopyroxene (n = 3) between 5.9 to 6.0 ‰, and olivine (n = 2) between 5.4 to 5.6 ‰. In gabbro, plagioclase (n = 2) has $\delta^{18}O$ values between 6.6 and 7.2 ‰ and clinopyroxene (n = 1) has 5.9 ‰. In gabbronorite, plagioclase (n = 2) ranges between 6.4 and 6.5 ‰ and the pyroxenes (undifferentiated due to similar oxygen isotope fraction factors: $\delta_{cpx-opx}$ < 0.1 [Kyser et al. 1981; Zheng 1993]) (n = 2) are 5.9 to 6.1 ‰. The xenolith plagioclase compositions fall within the range of plagioclase from volcanic rocks analysed by Druitt et al. [1999] ($\delta^{18}O$ = 5.7 to 7.5 ‰, Figure 9). The $\delta^{18}O$ values of melts in equilibrium with the xenolith mineral phases were calculated assuming the following fractionation factors: $\delta_{ol-melt}$ = −0.7 ‰, $\delta_{plag-melt}$ = 0.2 ‰, and $\delta_{pyx-melt}$ = −0.3 ‰ [Kyser et al. 1981; Kalamarides 1986; Harris et al. 2005]. The calculated melts cluster in $\delta^{18}O$ values between 6.1 and 6.5 ‰, with only one sample reaching a higher value of 7.0 ‰ (Figure 9).

5 DISCUSSION

The discussion will cover four major aspects of the formation of the plutonic xenoliths that provide additional insights into magma genesis at Santorini. First, the crystal cargo preserved in the plutonic xenoliths, based on mineral major and trace element compositions, is evaluated (Section 5.1). Second, the identification of exotic melt compositions based on

melt inclusion and mineral trace element contents is discussed (Section 5.2). Third, estimates for the intensive variables (P, T, fO_2) derived from the plutonic xenoliths is presented and compared to data from the volcanic products (Section 5.3). Finally, the role of crustal assimilation in the petrogenesis of the Santorini magmas is evaluated, focusing on the O-isotope evidence (Section 5.4).

5.1 Compositional trends and the presence of ancient xenocrysts

Major element whole rock, melt inclusion, and glass analyses from the xenoliths overlap with almost the entire compositional range of Santorini volcanic deposits for all major elements, generally following the typical liquid line of descent (Figure 7). Some xenolith whole-rock analyses deviate from the liquid line of descent, indicating a subtractive assemblage or cumulate origin [e.g. Morse 1976; Cooper et al. 2016; Melekhova et al. 2017]. The olivine gabbros and troctolites plot at low SiO_2 contents (46–49 wt%) and are considered to be the crystal fractionates that drive magmatic differentiation up to 58 wt% SiO_2 (Figure 7). Xenoliths with high Na_2O (> 6.5 wt%) between 59 and 65 wt% SiO_2 record the Na-rich plagioclase assemblage that drives inflection and differentiation to low Na_2O contents at greater than 68 wt% SiO_2 (Figure 7).

Although deep crustal amphibole-bearing cumulates are characteristic of many arcs worldwide, such as the Lesser Antilles [Arculus and Wills 1980; Tollan et al. 2012; Stamper et al. 2014; Cooper et al. 2016; Camejo-Harry et al. 2018], Andes [Costa et al. 2002], Japan[Tiepolo et al. 2012], and Solomon Islands [Smith 2014], primary amphibole is rare in the plutonic xenoliths from Santorini, only found as microlites within the olivine gabbro glass and rare interstitial crystals in the more evolved xenoliths [cf. Druitt et al. 1999]. The post-Akrotiri magmas at Santorini (<530 ka) are also characteristically amphibole-free and they show strong enrichment of Y with increasing differentiation (Figure 10). This trend reflects differentiation at shallow depths, which suppresses the importance of amphibole fractionation [Elburg et al. 2014]. Plutonic xenolith whole-rock compositions, glasses, melt inclusions and mineral compositions follow this amphibole-free differentiation trend (Figure 10), consistent with their anhydrous mineral assemblage. This geochemical similarity links the plutonic xenoliths to post-Akrotiri magma generation in shallow reservoirs. Only one gabbronorite xenolith, SAN 9-3-2
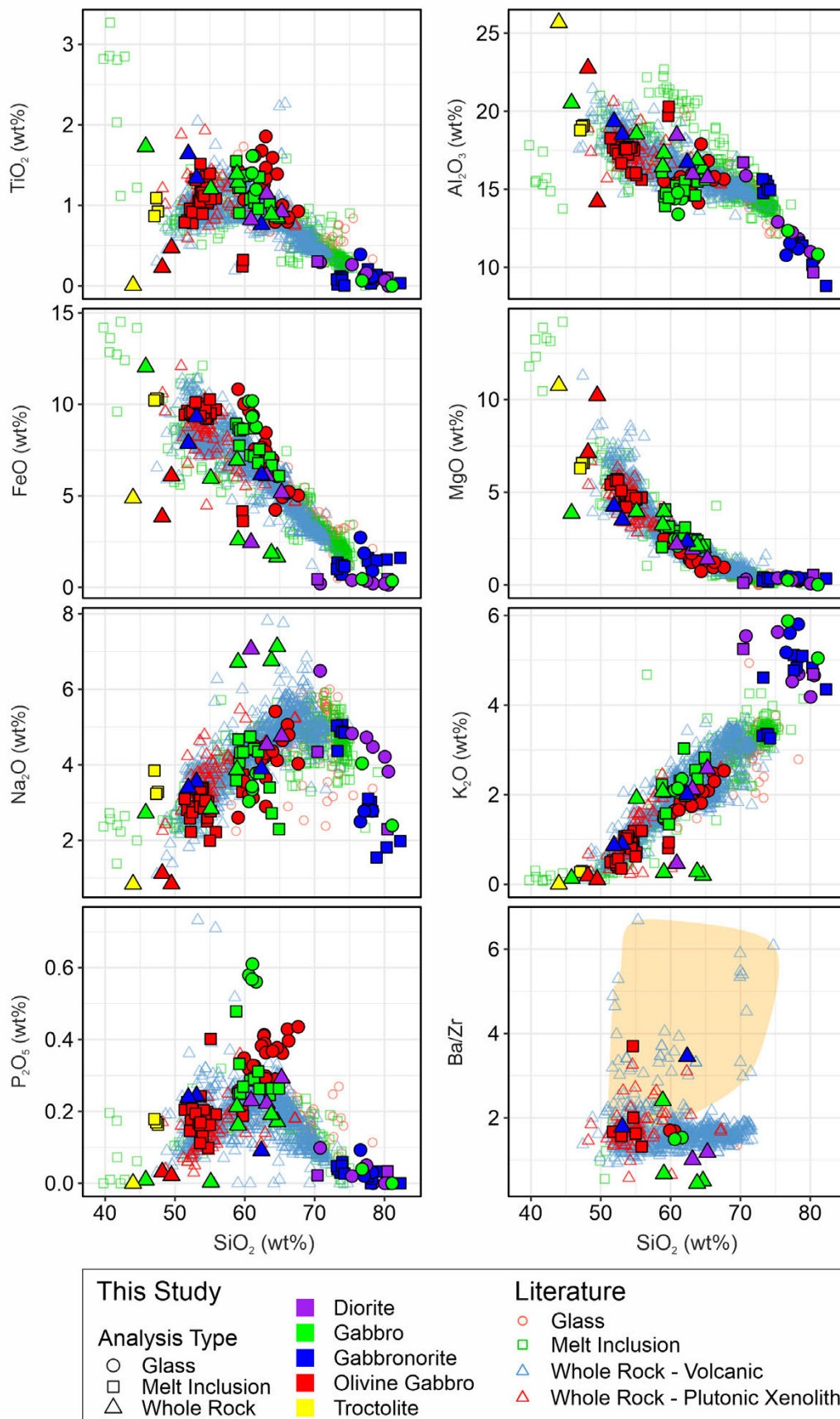
Figure 7: (Caption next page.)

Figure 7: (Previous page.) Whole rock, interstitial glass and melt inclusion compositions for xenoliths and volcanic rocks from the literature [GEOROC* (accessed 2017) Druitt 1983; Druitt et al. 1999; Michaud et al. 2000; Bailey et al. 2009; Gertisser et al. 2009; Panienka 2012; Fabbro et al. 2013; Elburg et al. 2014; Simmons et al. 2017]. Field of pre-530 ka volcanic deposits (Akrotiri) shown as light orange field on the Ba/Zr plot (see Section 5). Melt inclusion data comprise olivine, plagioclase and clinopyroxene hosted inclusions, and compositions shown are corrected for post entrapment modification, as discussed in Appendix A.2 (Supplementary Material 1). All major element values are normalised to 100 wt% volatile-free.

Table 2: Whole-rock compositions of Santorini xenoliths

	Analysis	XRF							
	Sample	SAN 4-4c	SAN 9-3-2	SAN 12-1-5	SAN 12-1-8-2	SAN 6-5-3	SAN 9-1-3	SAN 9-1-4	SAN 6-4-2
	Eruption	MIN	MIN	CR	US2	MP	LP2	LP2	LP1
	Rock type	Gabbro	Gabbronorite	Gabbronorite	Diorite	Diorite	Gabbro	Gabbro	Gabbro
Major elem. (wt%)	SiO_2	64.17	61.71	52.35	62.57	64.67	63.26	58.35	58.06
	TiO_2	0.85	0.75	1.32	1.13	0.91	0.88	1.27	1.37
	Al_2O_3	16.23	16.54	18.25	15.83	15.59	16.74	17.12	16.23
	Cr_2O_3								
	FeO	1.65	6.09	9.19	6.04	5.12	1.85	2.56	6.85
	MnO	0.02	0.12	0.16	0.16	0.14	0.03	0.04	0.10
	MgO	2.00	2.31	3.46	1.91	1.38	2.10	3.91	3.20
	CaO	6.92	5.50	9.27	4.65	3.71	7.12	8.53	6.74
	Na_2O	7.08	3.85	3.50	4.49	4.71	6.70	6.64	3.82
	K_2O	0.20	1.98	0.88	2.10	2.56	0.28	0.26	2.04
	P_2O_5	0.17	0.09	0.24	0.22	0.29	0.19	0.16	0.21
	Sum	99.29	98.94	98.62	99.10	99.08	99.15	98.84	98.62
Trace elem. (ppm)	Sc	17	18	29	17	13	14	26	22
	Sr	193	206	242	168	152	263	262	210
	Y	39	24	31	41	46	31	42	31
	Zr	215	154	78	252	288	298	122	130
	Nb	18	9	11	14	14	18	10	14
	Ba	108	532	139	254	340	133	82	313

	Analysis	Point count combined with averaged mineral and glass chemistry						
	Sample	SAN 5-2-1u	SAN 12-2-2	SAN 6-5-2-1	SAN 9-2-2	24D	28D	SAN 9-1-8-3
	Eruption	NK	US1	MP	MP	LP2	LP2	LP2
	Rock type	Troctolite	Gabbronorite	Olivine gabbro	Gabbro	Olivine gabbro	Diorite	Gabbro
Major elem. (wt%)	SiO_2	43.99	51.90	49.49	55.12	48.17	61.02	45.81
	TiO_2	0.01	1.64	0.47	1.20	0.23	0.82	1.73
	Al_2O_3	25.68	19.34	14.20	18.55	22.76	18.50	20.53
	Cr_2O_3	0.00	0.01	0.03	0.01	0.03	0.00	0.01
	FeO	4.88	7.87	6.08	5.96	3.85	2.46	12.04
	MnO	0.07	0.19	0.15	0.25	0.09	0.04	0.18
	MgO	10.77	4.26	10.22	3.96	7.14	2.19	3.88
	CaO	13.76	10.29	18.38	10.19	16.39	7.42	12.95
	Na_2O	0.84	3.39	0.84	2.84	1.12	7.08	2.72
	K_2O	0.00	0.87	0.11	1.91	0.19	0.46	0.13
	P_2O_5	0.00	0.24	0.02	0.00	0.03	0.23	0.01
	Sum	100.00	99.99	100.00	100.00	100.00	100.23	100.00

(Minoan eruption), falls within the amphibole-bearing differentiation trend, which is characterised by low and near-constant Y contents, suggesting that it is derived from earlier Akrotiri magmatic activity or a younger intrusion compositionally similar to the Akrotiri deposits [Druitt et al. 1999; Druitt 2014]. Along the Aegean arc, amphibole fractiona-

tion at greater depth from magmas with high water contents was invoked for both the early centres on Santorini (Akrotiri) and for Methana (up to 480 MPa [Elburg et al. 2014]), and amphibole-bearing cumulate rocks from Nisyros crystallised at even higher pressures of 500–800 MPa [Klaver et al. 2017]. In contrast to these rocks influenced by the presence of am-

Table 3: Oxygen isotope compositions (in $\delta^{18}O$ units) of the xenolith mineral phases

Sample	Rock type	Plagioclase	Olivine	Pyroxene[†]
SAN 9-1-8-1	Olivine gabbro	6.33	5.35	5.92
SAN 9-1-8-2	Olivine gabbro	6.34	5.63	6.00
SAN 6-3-1	Gabbro	7.20		
SAN 9-2-2	Gabbro	6.62		5.90
SAN 12-1-5	Gabbronorite	6.50		5.88
SAN 14-1-3-3	Gabbronorite	6.41		6.05

[†] Gabbronorite pyroxenes are undifferentiated ortho- and clinopyroxene, all other pyroxenes are clinopyroxene.

Figure 8: Glass and melt inclusion [A] REE and [B] trace element data (not corrected for PEC). The light grey lines are literature data for the volcanic rocks from GEOROC* (accessed 2017; see Lehnert et al. [2000]), Druitt et al. [1999], Bailey et al. [2009], Panienka [2012], Fabbro et al. [2013], Elburg et al. [2014], and Simmons et al. [2017]. Normalisation values from Palme and O'Neill [2014].

Two distinct groups of melt compositions have been identified at Santorini: Melts with high Ba and low Zr contents that formed the pre-530 ka Akrotiri volcanic complex and occur as intermediate rocks emplaced between 22 ka and 2.6 ka ('hornblende diorites' of Druitt [2014]), and the post-530 ka melts characterised by low Ba and high Zr concentrations [Druitt 2014]. Dominantly, the xenoliths in this study represent material derived from the post-530 ka low Ba/Zr magmas based on whole-rock Ba/Zr vs. SiO$_2$ relationships (Figure 7). The calculation of Ba and Zr contents for melts in equilibrium with the mineral phases [Bédard 2006; 2007; 2014] reveals that a small subset of crystals from xenoliths hosted in volcanic rocks older than the Minoan eruption have a high Ba and low Zr character (Figure 11A), suggesting that they represent xenocrysts inherited from the pre-530 ka Akrotiri magma.

Major element mineral compositions provide further evidence for the partial incorporation of a compositionally distinct crystal cargo into the xenoliths. The wide variety of xenoliths in the Lower Pumice 2 eruption allows a comparison of mineral compositions of volcanic [Gertisser et al. 2009] and xenolithic material (Figure 11B, C). Clinopyroxene from olivine gabbro and gabbro xenoliths overlaps with the compositional trend shown by crystals from mafic enclaves, suggesting a cogenetic origin. In contrast, diorite and gabbronorite clinopyroxenes plot below the expected compositional trend within the low Ti-Al clinopyroxene compositional group observed in xenoliths sampled from many eruptions (Figure 5B, C). This compositional group is not matched by any experimental clinopyroxenes synthesised from Santorini compositions [Cadoux et al. 2014; Andújar et al. 2015; 2016]. Instead, they are best matched by major element compositions (Al$_2$O$_3$, TiO$_2$, CaO; Figure 11B,C) of some hydrothermally altered clinopyroxenes [Manning and Bird 1986; Rose and Bird 1994; Good et al. 1997; Martinez-Serrano 2002; Marks et al. 2010], suggesting low Ti and Al as a way to identify hydrothermally altered clinopyroxenes. Hydrothermal alteration is pervasive in many xenoliths and cryptic alteration may have modified the mineral compositions without changing the pyroxenes fully to amphibole. For the Lower Pumice 2 eruption, the presence of fresh glass-bearing olivine gabbros and gabbros with compositions that match the volcanic deposits, and altered gabbronorites and diorites within the same deposit, indicate that the gabbronorites and diorites may be entrained fragments of altered fragments from a previous eruption or

phibole, but similar to the post-Akrotiri rocks on Santorini, a suite of low-porphyricity andesites from Nisyros was explained by differentiation at shallow levels (200–400 MPa) at moderate water contents (2–4 wt%), resulting in the absence of amphibole in the more primitive members of the suite (basaltic andesites and andesites) as amphibole phenocrysts only occur in the highly evolved dacites with high (>6 wt%) water contents [Klaver et al. 2017]. Evidently, the different depths of magmatic differentiation and differences in melt water content play a major role in defining the geochemical evolution at the various volcanic centres of the Aegean arc.
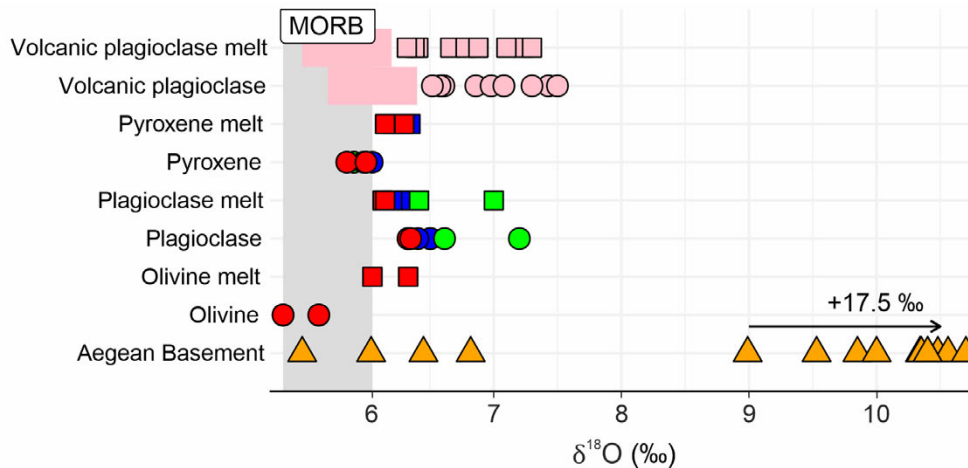
Figure 9: Oxygen isotope compositions of xenolith mineral phases, volcanic plagioclase and Aegean basement. The volcanic plagioclase points are pumice plagioclase phenocrysts from Druitt et al. [1999]. The pink fields are lava plagioclase phenocrysts from Wulf et al. [2020]. Aegean basement lithologies from Matthews and Schliestedt [1984], Bröcker et al. [1993], Putlitz et al. [2000], and McGrath et al. [2017] that may be considered potential contaminants of Santorini magmas. Calculated $\delta^{18}O$ of melts in equilibrium with the mineral phases are shown (see text for more detail) for comparison with typical MORB compositions [Ito et al. 1987]. The xenolith rock types are coloured as in Figures 5 and 6.
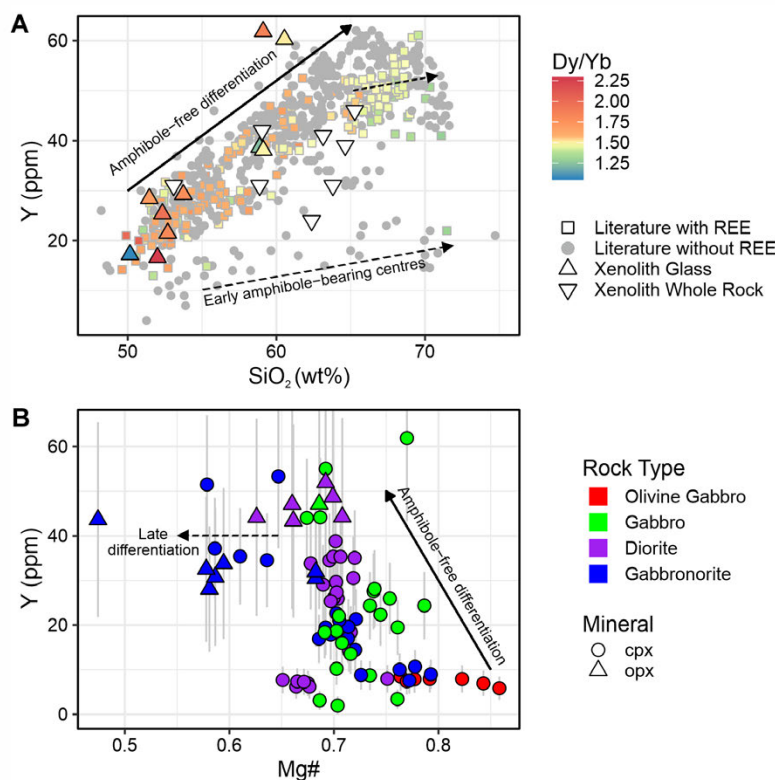
Figure 10: (Left) Geochemical tracers of amphibole fractionation applied to Santorini plutonic xenoliths. [A] Y vs SiO_2 variation at Santorini. Xenolith melt inclusion and interstitial glass (upwards triangles, coloured by Dy/Yb) and whole rock (downwards triangles) for comparison with literature data of volcanic rocks. The main trend for Santorini rocks (solid arrows) indicates amphibole-free differentiation. The influence of amphibole (flat trend for Y and decreasing Dy/Yb with increasing differentiation; dashed arrows) is only clear in the early amphibole-bearing centres (Akrotiri) and at >65 wt% SiO_2 at the latest evolutionary stage of the main trend. [B] Calculated melt Y in equilibrium with clinopyroxene and orthopyroxene against Mg# as a differentiation index. A similar trend to the Y vs SiO_2 diagram is shown, with increasing Y until an inflection at higher differentiation (lower Mg#). Uncertainty in Y equilibrium melt calculations are ~30 % and ~50 % for cpx and opx relative respectively [Bédard 2007; 2014].

intrusion [cf. Druitt et al. 1999], whilst the olivine gabbro and gabbros are samples from a crystallising Lower Pumice 2 crystal mush. Both the Ba/Zr data and the low Ti-Al clinopyroxenes show that not only a part of the xenolithic cargo in the eruptions may be derived from earlier non-cogenetic material, but even individual crystals could become entrained from older rocks and mixed into the magmatic system.

5.2   Evidence for exotic interstitial melt compositions

The diverse range of glass and melt inclusion compositions (47–82 wt% SiO_2) within the plutonic xenoliths record trapping of melts encompassing almost the entire magmatic history of Santorini. These compositions do not always closely follow the liquid line of descent and vary within individual samples. Major element and REE compositional data provide
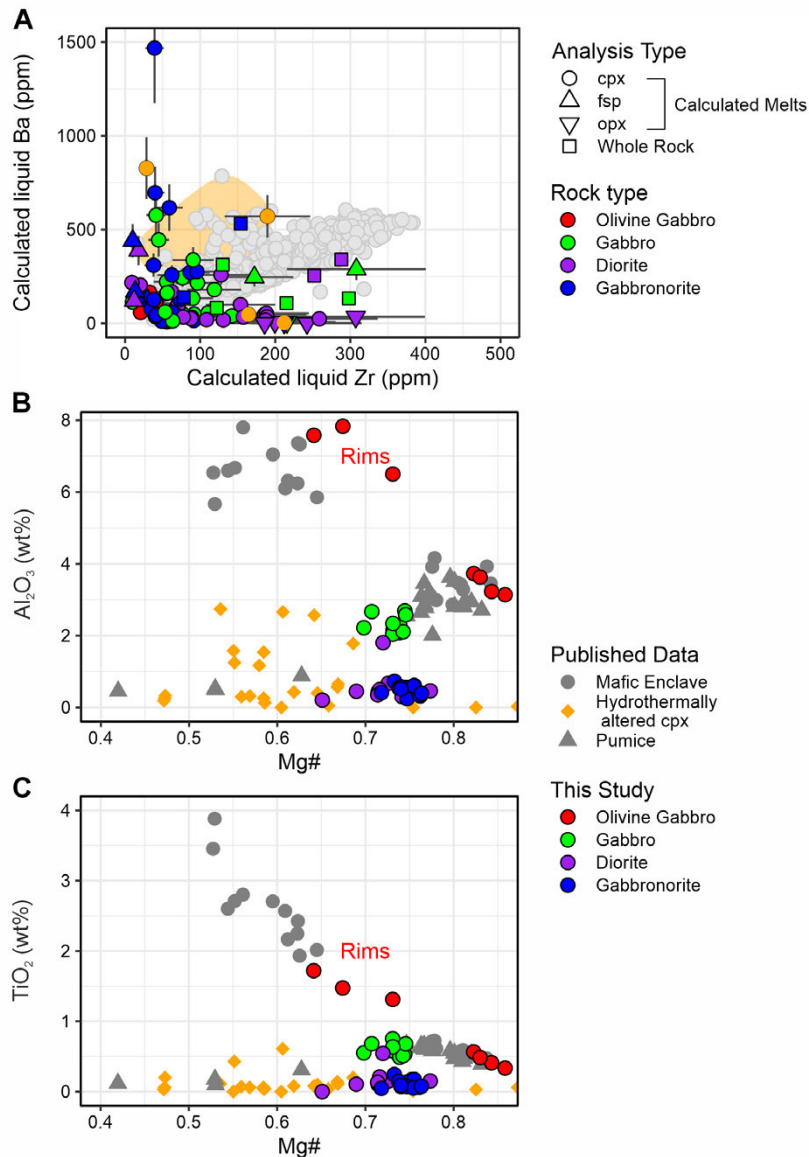
Figure 11: (Left) [A] Ba vs Zr plot highlighting the geochemical difference between the early Akrotiri volcanic deposits (orange field and points within) and later post-530 ka volcanic deposits (grey points). Literature data sources as in Figure 7. Melts calculated in equilibrium with xenolith clinopyroxene, orthopyroxene and plagioclase are shown (partition coefficients from Bédard [2006, 2007, 2014]), as well as xenolith whole rock data. Orange points represent melts in equilibrium with the Minoan gabbronorite (hornblende-diorite of Druitt [2014]). Equilibrium melt calculations introduce an uncertainty of about 30 %, as indicated by the error bars. [B] and [C] Comparison of Lower Pumice 2 phenocryst and xenolith clinopyroxene compositions. Data for clinopyroxene in volcanic rocks from Gertisser et al. [2009], Cadoux et al. [2014], and Druitt et al. [2016]. Hydrothermal clinopyroxene compositions from Manning and Bird [1986], Rose and Bird [1994], Good et al. [1997], Martinez-Serrano [2002], and Marks et al. [2010].

several lines of evidence for continued fractional crystallisation within the xenoliths that has produced differentiated melt compositions not preserved in the volcanic record:

(i) Mafic and intermediate (<65 wt% SiO_2) xenolith interstitial glass compositions have higher FeO, TiO_2, and P_2O_5 contents and lower Al_2O_3 contents compared to the liquid line of descent (Figure 7). Their compositional trend can be explained by predominant fractionation of plagioclase, which is the dominant interstitial mineral phase, lowering Al_2O_3 in the interstitial melt pockets with only subordinate effects of olivine and clinopyroxene fractionation.

(ii) Glass compositions are out of equilibrium with the ferro-magnesian phases based on Mg-Fe mineral-melt partition coefficients (e.g. $KD_{Fe-Mg}^{cpx-melt} = 0.23 - 0.28 \pm 0.06$; [Putirka 2008; Bédard 2010]) (Figure 12). Interstitial glass compositions are also more silicic (up to 82 wt% SiO_2) than unaltered volcanic whole-rocks. This is also shown by regressing the Santorini liquid line of descent Fe/Mg values against SiO_2 ($R^2 =$

0.75) and using $KD_{Fe-Mg}^{cpx-melt} = 0.23 - 0.28 \pm 0.06$ to estimate the SiO_2 of melts that would be in equilibrium with clinopyroxene. The maximum melt SiO_2 in equilibrium with xenolith clinopyroxene is ~70 ± 3 wt% SiO_2, lower than the range of 75 to 82 wt% SiO_2 commonly measured in the interstitial glasses.

(iii) The effects of continuing fractional crystallisation can be evaluated using equilibrium melt compositions calculated from clinopyroxene trace element data (Figure 13). For olivine gabbros and gabbros, the calculated melt trace elements and REE profiles generally overlap with volcanic whole-rock concentrations and glass compositions (Figure 13A), indicating that clinopyroxene crystallised from a typical mafic to intermediate Santorini melt. For those rocks, there is little evidence for prolonged fractional crystallisation recorded in the clinopyroxene trace element composition alone, although this may be sampling bias from mostly crystal core analyses. Melts calculated from clinopyroxene in gabbronorite and diorite xenoliths show highly variable patterns with compositions outside the

volcanic whole-rock field (Figure 13A). The progressive trace element enrichment with increasing crystallisation of the interstitial melt, exemplified in the decreasing Mg# from 79 to 56 in gabbronorite SAN 12-2-2, demonstrates that the trace element enrichment is controlled by fractional crystallisation of the interstitial melt. The important role of plagioclase fractional crystallisation is clearly reflected in the Eu anomaly in clinopyroxene, which is positively correlated with enrichment in REEs such as La (Figure 6D). Gabbronorite SAN 9-1-1-3 has a restricted Mg#$_{cpx}$ range between 76 and 72, yet the highest trace element enrichment of any xenolith and the largest Eu anomaly (Figures 6A, 13), indicating that clinopyroxene crystallisation occurred after feldspar fractionation.

This *in situ* trapped interstitial melt crystallisation has been recognised in layered intrusions and plutons to influence the chemical composition of residual melts, including increasing incompatible trace element concentrations, and of minerals that crystallise from or re-equilibrate with these late stage melts [e.g. Barnes 1986; Bédard 1994; Borghini and Rampone 2007]. To test if the melt REE compositions can be produced from fractional crystallisation of a Santorini melt, the REE concentrations during fractional crystallisation of a Santorini basalt (sample MVD-T 00-10 [Bailey et al. 2009]) were modelled over 3 steps [cf. Borghini and Rampone 2007]. The bulk partition coefficient (D) was estimated as 0.05 for the entire crystallisation, approximating a fractionating assemblage made up of plagioclase and pyroxene [Bédard 2006; 2007; Sun and Liang 2012; Bédard 2014; Sun et al. 2017], and a bulk D of 0.5 for Eu was used, based on the high modal proportion of plagioclase and large Eu anomalies in the xenolith mineral phases. A value of 0.05 was chosen for each element partition coefficient (except Eu) because although D_{REE} decreases with ionic radius in the pyroxenes [Bédard 2006; Sun and Liang 2012; Bédard 2014], it increases in plagioclase [Bédard 2007; Sun et al. 2017], essentially cancelling out the differences. For example, increasing the bulk D by 0.01 for each step from La to Lu produces strongly negative profile slopes, not observed in the xenolith clinopyroxene (Figure 6A, B). This simplified model does not account for the weak amphibole fractionation as noted for the more evolved REE profiles at Santorini and a changing mineral assemblage during differentiation (olivine first, Fe-Ti oxides and apatite later). However, as a first-order estimation, fractional crystallisation of a mineral assemblage comprising plagioclase and pyroxenes and a trapped interstitial melt can produce the full range of equilibrium melt REE patterns (Figure 13B) observed in the xenoliths.

A different but related explanation for the highly enriched clinopyroxene trace element compositions is re-equilibration with the crystallising interstitial melt. This 'trapped liquid shift' [Barnes 1986] drives ferromagnesian mineral compositions to iron enrichment and lower Mg# values. As both crystallisation from a trace element enriched melt and re-equilibration with this melt will ultimately produce a similar result of trace element enriched crystals, it is difficult to establish the exact process occurring. Since REE diffusion is slow in clinopyroxene [Van Orman et al. 2001], it should retain REE zonation from crystallisation as shown in sample SAN 12-2-2 (Figure 13B), where REE enrichment of clinopyroxene

rims relative to cores is thought to occur due to trapped melt crystallisation and subsequent REE enrichment. However, re-equilibration is apparent in gabbronorite samples that contain rare olivine (Fo$_{47-69}$) with a reaction rim and Fo values that are lower than in olivines from olivine gabbro and troctolites (Fo$_{74-84}$) and lava phenocrysts (Fo$_{68-93}$, Figure 5A). Temperature estimated from mineral-melt thermometry (see below) show re-equilibration at temperatures as low as 800 °C, either with the interstitial melt or with clinopyroxene and orthopyroxene in the same samples.

An alternative concept for melt differentiation involves reactions between the replenishing primitive melts and a crystal mush [e.g. Leuthold et al. 2014; Lissenberg and MacLeod 2016; Boulanger and France 2023]. This concept emphasises the importance of reactive porous flow for magma differentiation and it uses characteristic textures and *in situ* mineral compositions as evidence for melt-mush reactions [Boulanger and France 2023]. Although there is some textural evidence in the Santorini xenoliths that are consistent with reactive porous flow processes, such as rounded olivines enclosed in plagioclase in the troctolite glomerocrysts, the key characteristics of the mineral trace element contents are opposite to what would be expected if reactive porous flow was the main differentiation mechanism. In particular, REE concentrations and Eu anomalies in clinopyroxene systematically correlate with differentiation indices and rock type, and there is a systematic inverse correlation of incompatible trace elements with An content in plagioclase. These features are opposite to decoupling between major and trace elements in minerals expected from reactive porous flow processes [see Boulanger and France 2023, for details]. Moreover, the presence of interstitial albite-rich plagioclase, orthoclase, quartz, and apatite in the Santorini xenoliths is expected from the crystallisation of a highly differentiated trapped melt.

In summary, many xenoliths show evidence that the trapped interstitial melts are compositionally distinct to the erupted Santorini melts that produce the Santorini liquid line of descent. Extraction of melts at early stages of magmatic evolution are able to produce compositions comparable to the erupted Santorini magmas [cf. Flaherty et al. 2018], shown by melt inclusion compositions across the xenolith types generally overlapping with the liquid line of descent. More extensive fractionation in the interstitial melts of the Santorini xenoliths can produce unique compositions of the crystallising minerals. The evidence for melt compositional variability preserved in the plutonic xenoliths adds to the diversity of preserved melt compositions that starts with a range of primitive melt compositions measured in Mg-rich olivines (Fo ≥ 80), which occur due to changes in the fluxes of sediment melt or fluid and/or changes in the degree of melting [Flaherty et al. 2022].

5.3 Xenolith Intensive Variables and Magma Plumbing

To place constraints on the formation conditions of the xenoliths, we used thermobarometric models (see Appendix A.3 in Supplementary Material 1) and a comparison between xenolith minerals and experimental data [Cadoux et al. 2014; Andújar et al. 2015; 2016]. Olivine, plagioclase, orthopyroxene, and
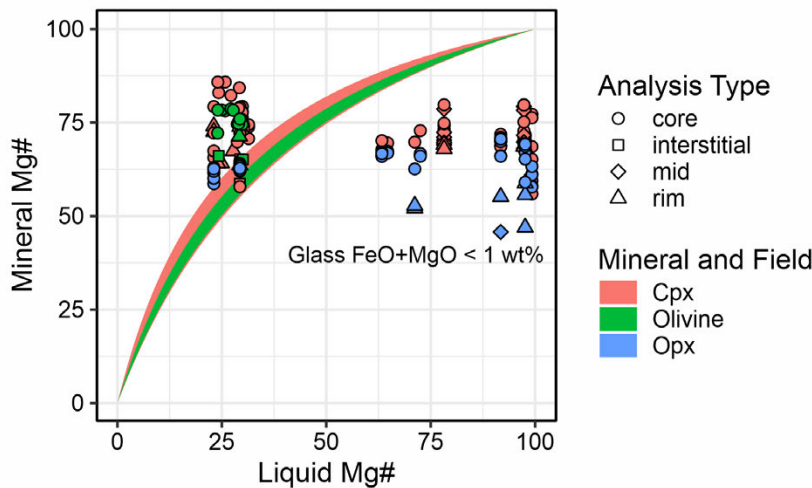
Figure 12: (Left) Evaluation of equilibrium between ferromagnesian minerals and interstitial melt. Equilibrium $K_D^{mineral-melt}$ fields are shown for olivine (green) and clinopyroxene (red).

Figure 13: (Right) Calculated melts in equilibrium with xenolith clinopyroxene compared to volcanic whole-rocks (light grey). [A] Average calculated melts in equilibrium with xenolith clinopyroxene in each sample. See the text for discussion on the choice of partition coefficients. [B] Two selected samples that show either a wide range of REE concentrations (SAN 12-2-2) or highly enriched compositions (SAN 9-1-1-3).
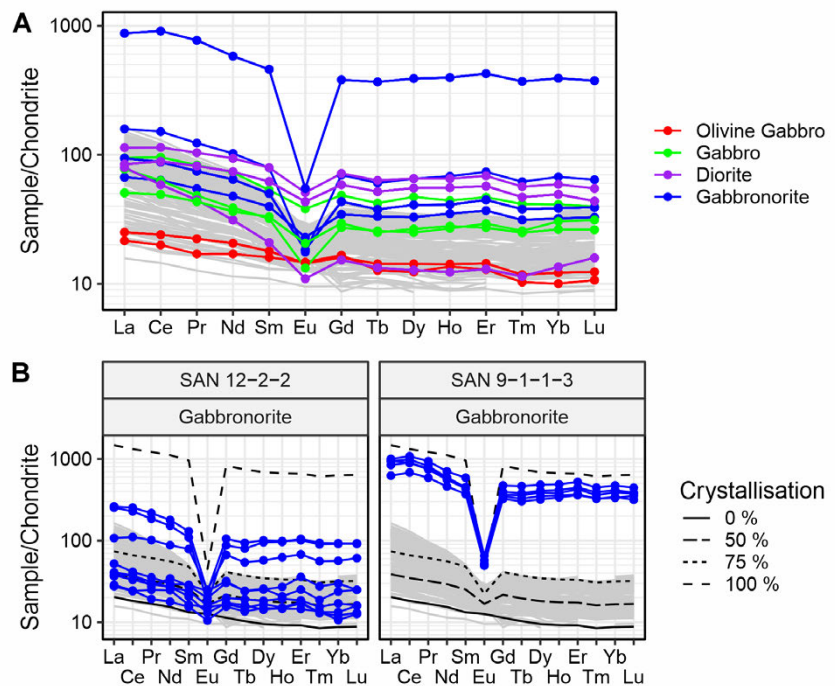
clinopyroxene thermobarometric models indicate that the entire xenolith suite formed at pressures <360 MPa (± 100 MPa model uncertainty), corresponding to depths of less than approximately 14 km when assuming a Santorini crustal density of 2640 kg m^{-3} [Konstantinou 2010] (see Figure 14). Olivine gabbro mineral cores record pressures of less than 200 ± 100 MPa, whilst the other lithologies span the full pressure range. Temperature and pressure estimates are generally positively correlated. Some clinopyroxene rim analyses produce higher pressure estimates than the cores, which are considered as spurious caused by rapid element uptake during cooling [Mollo et al. 2010] and are therefore not shown.

Temperature estimates range from 1124 ± 55 °C for plagioclase crystallisation in the troctolites to 731 ± 33 °C for rim and interstitial plagioclase in the gabbronorites. Individual samples can record a 200 °C variation between mineral core and rim/interstitial temperatures. The olivine gabbros and troctolites record the highest temperatures, and the gabbros, gabbronorites, and diorites generally overlap at a lower temperature range. There are temperature variations between thermometric results based on the different mineral phases (see Figure 14). Plagioclase temperatures record crystallisation throughout the entire differentiation history, consistent with petrography and major element geochemistry, from 1124 to 731 °C. Clinopyroxene crystallises over the 1063 to 893 °C temperature range, orthopyroxene between 1015 and 871 °C. Olivine crystallises between 1105 and 1010 °C and is found as texturally partially re-equilibrated rare xenocrysts in gabbronorites, recording lower re-equilibration temperatures between 960 and 796 °C. Oxygen isotope thermometry applied to the xenolith minerals also gives magmatic temperatures (Fig-

ure 15) that are in broad agreement with the mineral-melt derived temperatures.

A comparison between measured mineral compositions and compositions produced experimentally under controlled *P-T* conditions are useful to evaluate the results of the thermobarometric calculations and constrain crystallisation conditions [e.g. Halama et al. 2006; Andújar et al. 2016; Melekhova et al. 2017]. Comparisons of the compositions of the olivine gabbro mineral assemblage to experimental data of Andújar et al. [2015] match the 200–400 MPa 1040 °C experiments, consistent with the mineral-melt thermobarometry above. Andújar et al. [2016] found that Santorini melt FeO/MgO is controlled by the depth of crystallisation and found this parameter can be used as a geobarometer. A comparison between olivine gabbro and gabbro interstitial glass and melt inclusion FeO/MgO vs SiO_2 compositions to the experimental data of Andújar et al. [2015] and Andújar et al. [2016] also indicates pressures of 200–400 MPa. Gabbronorite melt inclusions match melts produced in experiments at 100–200 MPa.

The olivine gabbro xenoliths generally lack Fe-Ti oxides for estimating oxygen fugacity and temperature using two-oxide models, excluding micrometre-sized crystals of magnetite attached to the crystal rims at the contact with the interstitial glass. However, fO_2 can be estimated using the clinopyroxene-plagioclase-melt oxybarometer of France et al. [2010]. We have not used the France et al. [2010] model on more evolved lithologies as the interstitial glasses are not in equilibrium with the clinopyroxene. Pairings of mineral cores with melt inclusions, and rims with interstitial glass in the olivine gabbros and the glass-rich gabbro SAN 9-1-8-3 give values between NNO+1 to NNO+1.9 (1σ uncertainty on individual estimates is 0.7–2.28, 1σ uncertainty per sample is ±0.5) with no significant difference between core-melt inclusion and rim-interstitial glass. These estimates are close to the experimental estimates (NNO + 1) for Upper Scoria 1 andesitic magma [Andújar et al. 2016] and two oxide estimates for rhyodacitic magma (~NNO + 0.5 [Cottrell et al. 1999]), although higher than previously determined for mafic magmas from two oxide oxybarometry and experimental constraints (~QFM [Gertisser et al. 2009; Andújar et al. 2015]). Oxygen fugacity estimates for gabbros and gabbronorites based on two oxide oxybarometry (ILMAT [Lepage 2003]) indicate conditions of NNO −1 to +2 (Figure 14). Temperatures range from 903 to 605 °C. The lower values in this range of temperatures, combined with the high estimated oxygen fugacities, are likely a combination of both subsolidus storage of the xenoliths and/or hydrothermal alteration.

Pressures estimated from mineral-melt thermobarometry and comparison with experimental mineral and glass compositions indicate formation at pressures less than 400 MPa for the entire xenolith suite analysed, over a temperature range from 1124 to 749 °C (excluding Fe-Ti oxide temperatures) at a fO_2 of ~NNO −1 to +2. This shows a dominant role of upper to mid-crustal magmatic differentiation. Overlap between plutonic xenolith mineral compositions and volcanic phenocrysts [Druitt et al. 2016] and indicate that both form at shallow to mid-crustal depths from already partially differentiated mantle melts, consistent with experimental work [Andújar et al. 2015;

2016]. Ultramafic cumulates from the lower crust related to the parental mantle-derived melts have not yet been found at Santorini.

5.4 Crustal contamination constraints from plutonic xenoliths

Published bulk rock oxygen isotope compositions of Santorini volcanic rocks ($\delta^{18}O$ = 5.8 to 13.5 ‰; [Hoefs 1978; Druitt et al. 1999]) are variably affected by secondary weathering and hydration of glass in pumice, masking possible effects of crustal contamination. Mineral separates are much less susceptible to these secondary effects, showing a much more restricted range in $\delta^{18}O$ values compared to whole rocks, and allowing insights into the magma genesis. The range in $\delta^{18}O$ calculated for melts in oxygen isotopic equilibrium with the xenolith minerals is 6.1 to 7.0 ‰, and 12 out of 13 analyses have a range between 6.1 and 6.5 ‰ (Figure 9). These values and the overall $\delta^{18}O_{melt}$ average of 6.3 ± 0.2 ‰ are higher than for typical MORB basalts ($\delta^{18}O$ = 5.7 ± 0.3 ‰; [Ito et al. 1987; Harmon and Hoefs 1995]), but they are similar to $\delta^{18}O_{melt}$ (5.5–7.3 ‰) calculated from published $\delta^{18}O$ values of volcanic plagioclase [Wyers 1987; Druitt et al. 1999]. The calculated $\delta^{18}O_{melt}$ values are independent of the mineral analysed (based on olivine, $\delta^{18}O_{melt}$ = 6.2 ± 0.2 ‰; based on clinopyroxene, $\delta^{18}O_{melt}$ = 6.3 ± 0.1 ‰; based on plagioclase, $\delta^{18}O_{melt}$ = 6.4 ± 0.3 ‰), indicating equilibration at magmatic temperatures and equilibrium between the minerals analysed. Temperatures estimated from oxygen isotope fractionation [Zheng 1993] between the xenolith mineral phases also demonstrate oxygen isotope equilibration at magmatic temperatures (Figure 15). Calculated temperatures are 935 to 1300 °C (ol-plag and cpx-plag) for the olivine gabbro, 805 to 1310 °C (px-plag) for the gabbronorite, and 900 °C (cpx-plag) for the gabbro. There is no evidence of secondary alteration in the oxygen isotope data and therefore the values obtained from the plutonic xenoliths for olivine ($\delta^{18}O$ = 5.4-5.6 ‰), pyroxenes ($\delta^{18}O$ = 5.9-6.1 ‰) and plagioclase ($\delta^{18}O$ = 6.3–7.2 ‰) are interpreted as representing magmatic values. The lowest xenolith $\delta^{18}O_{melt}$ values are qualitatively consistent with small amounts of source contamination by the addition of small amounts (< 1–-2 wt%) of slab-derived fluid into the magma source as suggested for subduction zone magmas in general [Eiler et al. 2000], or by subducted sediment contributions to the melts [Francalanci and Zellmer 2019], or they may reflect small amounts of assimilation in a crustal magma reservoir even of the most primitive Santorini magmas [Barton et al. 1983]. The observed range in $\delta^{18}O_{melt}$ falls within the range predicted for extreme closed-system fractional crystallisation that can lead to an increase in $\delta^{18}O$ of up to about 1.3 to 2.0 ‰ in silicic magmas [Muehlenbachs and Byerly 1982; Eiler 2001], although more recent modelling of oxygen isotope effects in island arc magmas suggests that closed system fractional crystallisation from a basaltic to a silicic composition (75 wt% SiO_2) would increase $\delta^{18}O$ in the magma by less than 0.5 ‰ [Bindeman 2008]. Since most of the Santorini xenoliths with mafic to intermediate bulk compositions have $\delta^{18}O_{melt}$ values between 6.1 and 6.5 ‰, closed-system fractional crystallisation is sufficient to explain this limited range of 0.4 ‰
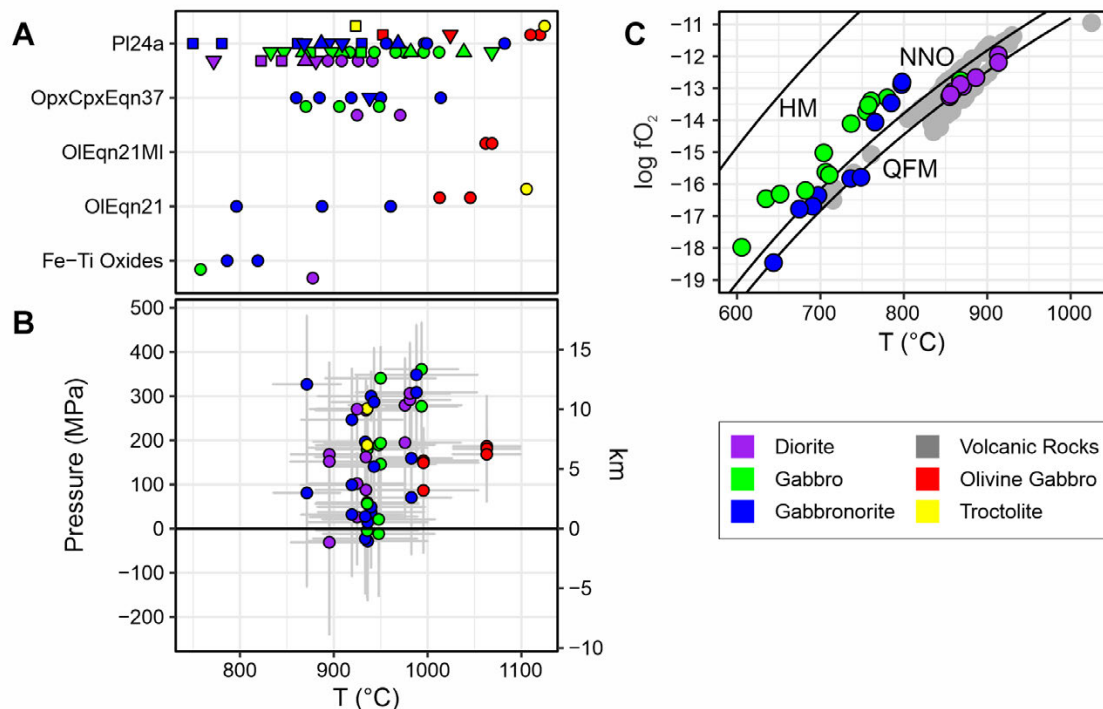
Figure 14: Thermobarometry of the Santorini xenoliths. Some models have been corrected to account for systematic overestimation at low pressure (as discussed in Appendix A.3, Supplementary Material 1). Model uncertainty bars are 1 standard deviation of the mean pressure or temperature calculated, which is generally less than the model uncertainty [Putirka 2008, cf.]. [A] the results from thermometric models that lack a reliable paired barometric equation. A pressure of 200 MPa is assumed. Temperatures vary <10 °C/100 MPa, which is insignificant in the 0 to 360 MPa range estimated from barometric models. [B] Results from Putirka [2008] equations clinopyroxene 31, 33, and 32b, orthopyroxene 29a and 29b, and the Neave and Putirka [2017] clinopyroxene barometer. Pressures estimated from crystal rims are not shown due to anomalously high (>600 MPa) and low (<200 MPa) estimates, possibly due to disequilibria resulting from fast cooling (Mollo et al. [2010]). Pressure estimates from the low Ti-Al clinopyroxene/orthopyroxene samples are not shown due to the negative pressures estimated. [C] Temperatures and oxygen fugacity estimated from coexisting magnetite and ilmenite pairs. Light grey literature values are Kameni dacite and diorite nodule values from Druitt [2014], Lower Pumice 2 pumice and mafic enclave values from Gertisser et al. [2009], and various pumice values from Panienka [2012] and Cadoux et al. [2014].

and does not require assimilation of crustal material. Only one xenolith sample may have been affected by minor crustal assimilation, although crustal contributions could be masked if contaminants have low $\delta^{18}O$ within the range of the igneous rocks. Small or negligible amounts of crustal assimilation in plutonic xenoliths, representing early stages of magmatic evolution, have been shown to be the case in Martinique (French Antilles) using Sr isotopes [Brown et al. 2021]. In contrast, more differentiated magmas from both Santorini [Briqueu et al. 1986; Druitt et al. 1999] and Martinique [Brown et al. 2021] do require combined assimilation and fractional crystallisation to explain more radiogenic Sr and Nd isotope compositions that are unlike compositions directly derived from typical mantle. Oxygen isotope compositions of plagioclase separates from the same volcanic rocks on Santorini are inconclusive, however, likely related to the non-distinct O-isotope composition of the assimilated material and/or the small amounts of it [Druitt et al. 1999]. The more radiogenic Sr-Nd isotope composition of the silicic melt compared to plagioclase phenocrysts suggests that the assimilation occurred at very shallow crustal levels immediately prior to eruption [Druitt et al. 1999]. This sce-

nario explains the lack of crustal assimilation in the plutonic xenoliths, which derive from greater depths in the magmatic plumbing system.

6   CONCLUSIONS

Plutonic xenoliths collected from across the stratigraphy of Santorini comprise troctolites, olivine gabbros, gabbros, diorites, and gabbronorites. Mineral compositions of the xenoliths generally overlap those of the volcanic phenocrysts but also extend to differentiation indices that demonstrate a higher degree of differentiation (low Fo in olivine, low X_{An} in feldspar, low Mg# in ferromagnesian silicates) in the respective interstitial melts. Melt inclusions record that the interstitial melts evolved towards exotic, more silica-rich compositions (up to 82 wt% SiO_2) not present in the volcanic record. Oxygen isotope compositions of olivine, pyroxenes, and plagioclase show equilibration at magmatic temperatures that are also compatible with the mineralogical compositions. Calculated $\delta^{18}O_{melt}$ values (6.1–7.0 ‰) are above typical values for MORB and consistent with extreme extents of fractionation at magmatic temperatures but permitting a small crustal
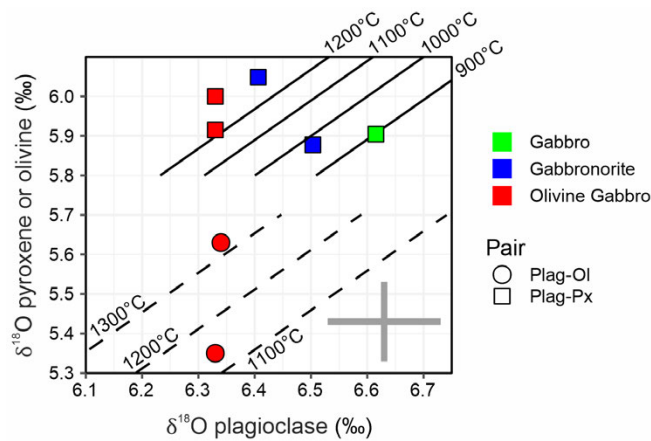
Figure 15: $\delta^{18}O$ values of xenolith pyroxene or olivine against coexisting plagioclase to assess mineral equilibration temperatures. Solid lines show isotherms of equilibrium pyroxene-plagioclase fractionation, and dashed lines show equilibrium isotherms of olivine-plagioclase fractionation (both after Zheng [1993]). Circles are pyroxene-plagioclase pairs and squares are olivine-plagioclase pairs. The cross indicates typical analytical uncertainty (1SD, ± 0.1 ‰).

contribution via slab fluids and/or crustal assimilation. Significant mineral trace element enrichment has been measured in some crystals, related to extensive fractional crystallisation or re-equilibration with trapped interstitial melts. Fractional crystallisation, predominantly of plagioclase, in the interstitial melts results in REE enrichment and increasing negative Eu anomalies in clinopyroxene crystals. The plutonic xenoliths hence preserve unique melt and mineral compositions that are not present in the volcanic record and provide additional insights into the magmatic system of Santorini. Remobilisation processes may cause disintegration of xenoliths causing crystals and trapped melts to mix into the magmatic system. On Santorini, the vast majority of plutonic xenoliths sampled derive from post-530 ka magmas and only rare, isolated crystals may have been derived from older magma batches. Some clinopyroxene crystals show geochemical characteristics of a preceding hydrothermal alteration. Thermobarometric calculations demonstrate that the entire xenolith suite is formed over a wide temperature range between 1100 to 750 °C, at shallow to mid crustal depths (< 400 MPa) from a partially differentiated primitive mantle melt. This shallow magma differentiation at Santorini largely inhibits amphibole fractionation, in contrast to Nisyros and Methana to the east and west within the South Aegean Volcanic Arc, respectively. This study of the Santorini plutonic xenoliths helps understand the complex processes occurring globally during arc magma petrogenesis [Andújar et al. 2016].

Author Contributions

RG and RH designed the study. SW, RG and RH collected the samples. SW performed the petrographic characterisation, mineral chemical analyses and thermobarometric calculations. THH and MF supervised the LA-ICP-MS analyses, TV contributed the oxygen isotope analyses. SW and RH drafted the

manuscript. All authors discussed the results and contributed to the final manuscript.

Data Availability

New data are presented in Tables 1–3. Additionally, supplementary information appearing alongside this article contains detailed information about analytical methods, post-entrapment crystallisation (PEC) corrections for melt inclusions, thermobarometric calculations, and calculations of trace element partition coefficients in Supplementary Material 1 as well as new electron microprobe and laser ICP-MS data in Supplementary Material 2.

Copyright notice

References

Andújar, J., B. Scaillet, M. Pichavant, and T. H. Druitt (2015). "Differentiation conditions of a basaltic magma from Santorini, and its bearing on the production of andesite in arc settings". *Journal of Petrology* 56, pages 765–794. DOI: 10.1093/petrology/egv016.

– (2016). "Generation Conditions of Dacite and Rhyodacite via the Crystallization of an Andesitic Magma. Implications for the Plumbing System at Santorini (Greece) and the Origin of Tholeiitic or Calc-alkaline Differentiation Trends in Arc Magmas". *Journal of Petrology* 57, pages 1887–1920. DOI: 10.1093/petrology/egw061.

Angelier, J., N. Lybéris, X. Le Pichon, E. Barrier, and P. Huchon (1982). "The tectonic development of the Hellenic arc and the Sea of Crete: a synthesis". *Tectonophysics* 86, pages 159–196. DOI: 10.1016/0040-1951(82)90066-X.

Arculus, R. and K. Wills (1980). "The petrology of plutonic blocks and inclusions from the Lesser Antilles island arc". *Journal of Petrology* 21, pages 743–799. DOI: 10.1093/petrology/21.4.743.

Bailey, J., E. Jensen, A. Hansen, A. Kann, and K. Kann (2009). "Formation of heterogeneous magmatic series beneath North Santorini, South Aegean island arc". *Lithos* 110, pages 20–36. DOI: 10.1016/j.lithos.2008.12.002.

Barnes, S. (1986). "The effect of trapped liquid crystallization on cumulus mineral compositions in layered intrusions". *Contributions to Mineralogy and Petrology* 93, pages 524–531. DOI: 10.1007/BF00371722.

Barton, M. and J. Huijsmans (1986). "Post-caldera dacites from the Santorini volcanic complex, Aegean Sea, Greece: an example of the eruption of lavas of near-constant composition over a 2,200 year period". *Contributions to Mineralogy and Petrology* 94, pages 472–495. DOI: 10.1007/BF00376340.

Barton, M., V. Salters, and J. Huijsmans (1983). "Sr isotope and trace element evidence for the role of continental crust in calc-alkaline volcanism on Santorini and Milos, Aegean Sea, Greece". *Earth and Planetary Science Letters* 63, pages 273–291. DOI: 10.1016/0012-821X(83)90042-0.

Beard, J. (1986). "Characteristic mineralogy of arc-related cumulate gabbros: implications for the tectonic setting of gabbroic plutons and for andesite genesis". *Geology* 14, pages 848–851. DOI: 10.1130/0091-7613(1986)14<848:CMOARC>2.0.CO;2.

Bédard, J. H. (1994). "A procedure for calculating the equilibrium distribution of trace elements among the minerals of cumulate rocks, and the concentration of trace elements in the coexisting liquids". *Chemical Geology* 118, pages 143–153. DOI: 10.1016/0009-2541(94)90173-2.

– (2006). "Trace element partitioning in plagioclase feldspar". *Geochimica et Cosmochimica Acta* 70, pages 3717–3742. DOI: 10.1016/j.gca.2006.05.003.

– (2007). "Trace element partitioning coefficients between silicate melts and orthopyroxene: parameterizations of D variations". *Chemical Geology* 244, pages 263–303. DOI: 10.1016/j.chemgeo.2007.06.019.

– (2010). "Parameterization of the Fe = Mg exchange coefficient (Kd) between clinopyroxene and silicate melts". *Chemical Geology* 274, pages 169–176. DOI: 10.1016/j.chemgeo.2010.04.003.

– (2014). "Parameterizations of calcic clinopyroxene—Melt trace element partition coefficients". *Geochemistry, Geophysics, Geosystems* 15, pages 303–336. DOI: 10.1002/2013GC005112.

Bindeman, I. (2008). "Oxygen isotopes in mantle and crustal magmas as revealed by single crystal analysis". *Reviews in Mineralogy and Geochemistry* 69, pages 445–478. DOI: 10.2138/rmg.2008.69.12.

Borghini, G. and E. Rampone (2007). "Postcumulus processes in oceanic-type olivine-rich cumulates: The role of trapped melt crystallization versus melt/rock interaction". *Contributions to Mineralogy and Petrology* 154, pages 619–633. DOI: 10.1007/s00410-007-0217-5.

Boulanger, M. and L. France (2023). "Cumulate formation and melt extraction from mush-dominated magma reservoirs: The melt flush process exemplified at mid-ocean ridges". *Journal of Petrology* 64, pages 1–20. DOI: 10.1093/petrology/egad005.

Briqueu, L., M. Javoy, J. Lancelot, and M. Tatsumoto (1986). "Isotope geochemistry of recent magmatism in the Aegean arc: Sr, Nd, Hf, and O isotopic ratios in the lavas of Milos and Santorini - geodynamic implications". *Earth and Planetary Science Letters* 497, pages 169–180. DOI: 10.1016/0012-821X(86)90018-X.

Bröcker, M., H. Kreuzer, A. Matthews, and M. Okrusch (1993). "40Ar/39Ar and oxygen isotope studies of polymetamorphism from Tinos Island, Cycladic blueschist belt, Greece". *Journal of Metamorphic Geology* 11, pages 223–240. DOI: 10.1111/j.1525-1314.1993.tb00144.x.

Brown, J., G. Cooper, G. Nowell, C. Macpherson, I. Neill, and J. Prytulak (2021). "Isotopic compositions of plagioclase from plutonic xenoliths reveal crustal assimilation below Martinique, Lesser Antilles Arc". *Frontiers in Earth Science* 9, page 682583. DOI: 10.3389/feart.2021.682583.

Cabato, E. J. A. (2007). "Abundances of Lithium, Beryllium and Boron in Phenocrysts from Santorini Volcano (Greece): Implications on Magma Genesis and Eruption Mechanisms". PhD thesis. University of Heidelberg. DOI: 10.11588/heidok.00007305.

Cadoux, A., B. Scaillet, T. H. Druitt, and E. Deloule (2014). "Magma storage conditions of large Plinian eruptions of Santorini Volcano (Greece)". *Journal of Petrology* 55, pages 1129–1171. DOI: 10.1093/petrology/egu021.

Camejo-Harry, M., E. Melekhova, J. Blundy, W. Attridge, R. Robertson, and T. Christopher (2018). "Magma evolution beneath Bequia, Lesser Antilles, deduced from petrology of lavas and plutonic xenoliths". *Contributions to Mineralogy and Petrology* 173, page 77. DOI: 10.1007/s00410-018-1504-z.

Chadwick, J., V. Troll, T. Waight, F. van der Zwan, and L. Schwarzkopf (2013). "Petrology and geochemistry of igneous inclusions in recent Merapi deposits: a window into the sub-volcanic plumbing system". *Contributions to Mineralogy and Petrology* 165, pages 259–282. DOI: 10.1007/s00410-012-0808-7.

Cooper, G., J. Blundy, C. Macpherson, M. Humphreys, and J. Davidson (2019). "Evidence from plutonic xenoliths from magma differentiation, mixing and storage in a volatile-rich crystal mush beneath St. Eustatius, Lesser Antilles". *Contributions to Mineralogy and Petrology* 174, page 39. DOI: 10.1007/s00410-019-1576-4.

Cooper, G., J. Davidson, and J. Blundy (2016). "Plutonic xenoliths from Martinique, Lesser Antilles: evidence for open system processes and reactive melt flow in island arc crust". *Contributions to Mineralogy and Petrology* 171, page 87. DOI: 10.1007/s00410-016-1299-8.

Costa, F., M. Dungan, and B. Singer (2002). "Hornblende-and phlogopite-bearing gabbroic xenoliths from Volcán San Pedro (36 S), Chilean Andes: evidence for melt and fluid migration and reactions in subduction-related plutons". *Journal of Petrology* 43, pages 219–241. DOI: 10.1093/petrology/43.2.219.

Cottrell, E., J. Gardner, and M. Rutherford (1999). "Petrologic and experimental evidence for the movement and heating of the pre-eruptive Minoan rhyodacite (Santorini, Greece)". *Contributions to Mineralogy and Petrology* 135, pages 315–331. DOI: 10.1007/s004100050514.

Davidson, J., S. Turner, H. Handley, C. Macpherson, and A. Dosseto (2007). "Amphibole "sponge" in arc crust?" *Geology* 35, pages 787–790. DOI: 10.1130/G23637A.1.

Davis, E. and C. Bastas (1978). "Petrology and geochemistry of the metamorphic system of Santorini". *Thera and the Aegean World.* Cambridge University Press, page 61.

Davis, E., E. Gartzos, and V. Dietrich (1998). "Magmatic evolution of the Pleistocene Akrotiri volcanoes". *Proceedings of the 2nd Workshop, "The European Laboratory Volcanoes," Santorini*, pages 2–4.

Dietrich, V. J., E. Davis, and E. Gartzos (1998). "Amphibole in rhyodacites and dacites from the Akrotiri volcanoes and the complexities of discontinuous fractional crystallization". *Proceedings of the 2nd Workshop, "The European Laboratory Volcanoes," Santorini*, pages 2–4.

Druitt, T. H. (1983). "Explosive volcanism on Santorini, Greece". PhD thesis. University of Cambridge.

– (2014). "New insights into the initiation and venting of the Bronze-Age eruption of Santorini (Greece), from component analysis". *Bulletin of Volcanology* 76, pages 1–21. DOI: 10.1007/s00445-014-0794-x.

Druitt, T. H., F. Costa, E. Deloule, M. Dungan, and B. Scaillet (2012). "Decadal to monthly timescales of magma transfer and reservoir growth at a caldera volcano". *Nature* 482, pages 77–80. DOI: 10.1038/nature10706.

Druitt, T. H., L. Edwards, R. Mellors, D. Pyle, R. Sparks, M. Lanphere, M. Davies, and B. Barriero (1999). *Santorini volcano*. Volume 19. Geological Society Memoir.

Druitt, T. H., R. Mellors, D. Pyle, and R. Sparks (1989). "Explosive volcanism on Santorini, Greece". *Geological Magazine* 126, pages 95–126. DOI: 10.1017/S0016756800006270.

Druitt, T. H., M. Mercier, L. Florentin, E. Deloule, N. Cluzel, T. Flaherty, E. Médard, and A. Cadoux (2016). "Magma storage and extraction associated with plinian and interplinian activity at Santorini caldera (Greece)". *Journal of Petrology* 57, pages 461–494. DOI: 10.1093/petrology/egw015.

Druitt, T. H., D. M. Pyle, and T. A. Mather (2019). "Santorini volcano and its plumbing system". *Elements* 15, pages 177–184. DOI: 10.2138/gselements.15.3.177.

Edwards, L. (1994). "Magma cyclicity and isotopic variation on Santorini volcano, Aegean Sea, Greece". PhD thesis. University of Bristol.

Eiler, J. (2001). "Oxygen isotope variations of basaltic lavas and upper mantle rocks". *Reviews in Mineralogy and Geochemistry* 43, pages 319–364. DOI: 10.2138/gsrmg.43.1.319.

Eiler, J., A. Crawford, T. Elliott, K. Farley, J. Valley, and E. Stolper (2000). "Oxygen isotope geochemistry of oceanic-arc lavas". *Journal of Petrology* 41, pages 229–256. DOI: 10.1093/petrology/41.2.229.

Elburg, M., I. Smet, and E. De Pelsmaeker (2014). "Influence of source materials and fractionating assemblage on magmatism along the Aegean Arc, and implications for crustal growth". *Geological Society, London, Special Publications*. Volume 385, pages 137–160. DOI: 10.1144/SP385.1.

Fabbro, G., T. H. Druitt, and S. Scaillet (2013). "Evolution of the crustal magma plumbing system during the build-up to the 22-ka caldera-forming eruption of Santorini (Greece)". *Bulletin of Volcanology* 75, pages 1–22. DOI: 10.1007/s00445-013-0767-5.

Fabbro, G. N., T. H. Druitt, and F. Costa (2018). "Storage and eruption of silicic magma across the transition from dominantly effusive to caldera-forming states at an arc volcano (Santorini, Greece)". *Journal of Petrology* 58, pages 2429–2464. DOI: 10.1093/petrology/egy013.

Flaherty, T., T. H. Druitt, L. Francalanci, P. Schiano, and O. Sigmarsson (2022). "Temporal variations in the diversity of primitive melts supplied to the Santorini silicic magmatic system and links to lithospheric stresses". *Contributions to Mineralogy and Petrology* 177, page 79. DOI: 10.1007/s00410-022-01941-6.

Flaherty, T., T. H. Druitt, H. Tuffen, M. Higgins, F. Costa, and A. Cadoux (2018). "Multiple timescale constraints for high-flux magma chamber assembly prior to the Late Bronze Age eruption of Santorini (Greece)". *Contributions to Mineralogy and Petrology* 173, page 75. DOI: 10.1007/s00410-018-1490-1.

Fouqué, F. (1879). *Santorini et ses éruptions*. Paris: Masson et Cie.

Francalanci, L. and G. Zellmer (2019). "Magma genesis at the South Aegean volcanic arc". *Elements* 15, pages 165–170. DOI: 10.2138/gselements.15.3.165.

France, L., B. Ildefonse, J. Koepke, and F. Bech (2010). "A new method to estimate the oxidation state of basaltic series from microprobe analyses". *Journal of Volcanology and Geothermal Research* 189, pages 340–346. DOI: 10.1016/j.jvolgeores.2009.11.023.

Gertisser, R., K. Preece, and J. Keller (2009). "The Plinian Lower Pumice 2 eruption, Santorini, Greece: magma evolution and volatile behaviour". *Journal of Volcanology and Geothermal Research* 186, pages 387–406. DOI: 10.1016/j.jvolgeores.2009.07.015.

Good, D., J. Crocket, and R. Barnett (1997). "A secondary clinopyroxene-chlorite-spinel assemblage in clinopyroxenite of the Mann complex, Abitibi Belt, Ontario: An unusual hydrothermal alteration suite". *Mineralogy and Petrology* 59, pages 69–90. DOI: 10.1007/BF01163062.

Halama, R., G. Boudon, B. Villemant, J.-L. Joron, A. Le Friant, and J.-C. Komorowski (2006). "Pre-eruptive crystallization conditions of mafic and silicic magmas at the Plat Pays volcanic complex, Dominica (Lesser Antilles)". *Journal of Volcanology and Geothermal Research* 153, pages 200–220. DOI: 10.1016/j.jvolgeores.2005.12.001.

Harmon, R. and J. Hoefs (1995). "Oxygen isotope heterogeneity of the mantle deduced from global 18O systematics of basalts from different geotectonic settings". *Contributions to Mineralogy and Petrology* 120, pages 95–114. DOI: 10.1007/BF00311010.

Harris, C., J. Pronost, L. Ashwal, and R. Cawthorn (2005). "Oxygen and hydrogen isotope stratigraphy of the Rustenburg Layered Suite, Bushveld Complex: constraints on crustal contamination". *Journal of Petrology* 46, pages 579–601. DOI: 10.1093/petrology/egh089.

Hawthorne, F., R. Oberti, G. Harlow, W. Maresch, R. Martin, J. Schumacher, and M. Welch (2012). "Nomenclature of the amphibole supergroup". *American Mineralogist* 97, pages 2031–2048. DOI: 10.2138/am.2012.4276.

Hoefs, J. (1978). "Oxygen isotope composition of volcanic rocks from Santorini and Christiani". *Thera and the Aegean World.* Edited by C. Doumas. Volume I. London: Aris & Phillips Ltd., pages 163–170.

Holness, M., M. Humphreys, R. Sides, R. Helz, and C. Tegner (2012). "Toward an understanding of disequilibrium dihedral angles in mafic rocks". *Journal of Geophysical Research* 117, B06207. DOI: 10.1029/2011JB008902.

Huijsmans, J., M. Barton, and V. Salters (1988). "Geochemistry and evolution of the calc-alkaline volcanic complex of Santorini, Aegean Sea, Greece". *Journal of Volcanology and Geothermal Research* 34, pages 283–306. DOI: 10.1016/0377-0273(88)90039-X.

Huijsmans, J. (1985). "Calc-alkaline lavas from the volcanic complex of Santorini, Aegean Sea, Greece: a petrological, geochemical and stratigraphic study". PhD thesis. Instituut voor Aardwetenschappen Rijksuniversiteit Utrecht.

Ito, E., W. White, and C. Göpel (1987). "The O, Sr, Nd and Pb isotope geochemistry of MORB". *Chemical Geology* 62, pages 157–176. DOI: 10.1016/0009-2541(87)90083-0.

Jackson, J. (1994). "Active tectonics of the Aegean region". *Annual Review of Earth and Planetary Sciences* 22, pages 239–271. DOI: 10.1146/annurev.ea.22.050194.001323.

Kalamarides, R. (1986). "High-temperature oxygen isotope fractionation among the phases of the Kiglapait intrusion, Labrador, Canada". *Chemical Geology* 58, pages 303–310. DOI: 10.1016/0168-9622(86)90018-7.

Karátson, D., R. Gertisser, T. Telbisz, V. Vereb, X. Quidelleur, T. H. Druitt, P. Nomikou, and S. Kósik (2018). "Towards reconstruction of the lost Late Bronze Age intra-caldera island of Santorini, Greece". *Scientific reports* 8, page 7026. DOI: 10.1038/s41598-018-25301-2.

Kilias, A., D. Mountrakis, M. Tranos, and S. Pavlides (1998). "The pre-volcanic metamorphic rocks of Santorini Island: Structural evolution and kinematics during the Tertiary (South Aegean, Greece)". *European Laboratory Volcanoes, Proc. 2nd Workshop on Europ. Lab. Volcanoes.* Edited by G. S. R. Casale M. Fytikas and G. Vougioukalakis. Europ. Comm., Sci. Res. Develop., pages 23–36.

Klaver, M., S. Carey, P. Nomikou, I. Smet, A. Godelitsas, and P. Vroon (2016). "A distinct source and differentiation history for Kolumbo submarine volcano, Santorini volcanic field, Aegean arc". *Geochemistry, Geophysics, Geosystems* 17, pages 3254–3273. DOI: 10.1002/2016GC006398.

Klaver, M., S. Matveev, J. Berndt, C. Lissenberg, and P. Vroon (2017). "A mineral and cumulate perspective to magma differentiation at Nisyros volcano, Aegean arc". *Contributions to Mineralogy and Petrology* 172, page 95. DOI: 10.1007/s00410-017-1414-5.

Konstantinou, K. (2010). "Crustal rheology of the Santorini–Amorgos zone: Implications for the nucleation depth and rupture extent of the 9 July 1956 Amorgos earthquake, southern Aegean". *Journal of Geodynamics* 50, pages 400–409. DOI: 10.1016/j.jog.2010.05.002.

Kyser, T., J. O'Neil, and I. Carmichael (1981). "Oxygen isotope thermometry of basic lavas and mantle nodules". *Contributions to Mineralogy and Petrology* 77, pages 11–23. DOI: 10.1007/BF01161498.

Lacroix, A. (1900). "Sur les transformations endomorphiques de la andesite de Santorini sous l'influence d'enclaves enallogènes calcaires". *Comptes rendus hebdomadaires des séances de l'Académie des sciences* 130, page 272.

Le Pichon, X. and J. Angelier (1979). "The Hellenic arc and trench system: a key to the neotectonic evolution of the eastern Mediterranean area". *Tectonophysics* 60, pages 1–42. DOI: 10.1016/0040-1951(79)90131-8.

Lehnert, K., Y. Su, C. H. Langmuir, B. Sarbas, and U. Nohl (2000). "A global geochemical database structure for rocks". *Geochemistry, Geophysics, Geosystems* 1(5). DOI: 10.1029/1999gc000026.

Lepage, L. (2003). "ILMAT: an excel worksheet for ilmenite–magnetite geothermometry and geobarometry". *Computers & Geosciences* 29, pages 673–678. DOI: 10.1016/S0098-3004(03)00042-6.

Leuthold, J., J. Blundy, M. Holness, and R. Sides (2014). "Successive episodes of reactive liquid flow through a layered intrusion (Unit 9, Rum Eastern Layered Intrusion, Scotland)". *Contributions to Mineralogy and Petrology* 168, page 1021. DOI: 10.1007/s00410-014-1021-7.

Lissenberg, C. and C. MacLeod (2016). "A reactive porous flow control on mid-ocean ridge magmatic evolution". *Journal of Petrology* 57, pages 2195–2220. DOI: 10.1093/petrology/egw074.

Locock, A. (2014). "An Excel spreadsheet to classify chemical analyses of amphiboles following the IMA 2012 recommendations". *Computers & Geosciences* 62, pages 1–11. DOI: 10.1016/j.cageo.2013.09.011.

Manning, C. and D. Bird (1986). "Hydrothermal clinopyroxenes of the Skaergaard intrusion". *Contributions to Mineralogy and Petrology* 92, pages 437–447. DOI: 10.1007/BF00374426.

Marks, N., P. Schiffman, R. Zierenberg, H. Franzson, and G. Fridleifsson (2010). "Hydrothermal alteration in the Reykjanes geothermal system: Insights from Iceland deep drilling program well RN-17". *Journal of Volcanology and Geothermal Research* 189, pages 172–190. DOI: 10.1016/j.jvolgeores.2009.10.018.

Martin, V., M. Holness, and D. Pyle (2006). "Textural analysis of magmatic enclaves from the Kameni Islands, Santorini, Greece". *Journal of Volcanology and Geothermal Research* 154, pages 89–102. DOI: 10.1016/j.jvolgeores.2005.09.021.

Martinez-Serrano, R. (2002). "Chemical variations in hydrothermal minerals of the Los Humeros geothermal system, Mexico". *Geothermics* 31, pages 579–612. DOI: 10.1016/S0375-6505(02)00015-9.

Matthews, A. and M. Schliestedt (1984). "Evolution of the blueschist and greenschist facies rocks of Sifnos, Cyclades, Greece". *Contributions to Mineralogy and Petrology* 88, pages 150–163. DOI: 10.1007/BF00371419.

McGrath, A., C. Stouraiti, and B. Windley (2017). "Geochemistry of mylonitic gneisses from the Cycladic Basement Unit (Paros and Serifos, Aegean Sea): implications for protoliths of the high-grade gneisses". *International Journal of Earth Sciences* 106, pages 2067–2089. DOI: 10.1007/s00531-016-1414-0.

Melekhova, E., J. Blundy, R. Martin, R. Arculus, and M. Pichavant (2017). "Petrological and experimental evidence for differentiation of water-rich magmas beneath St. Kitts, Lesser Antilles". *Contributions to Mineralogy and Petrology* 172, page 98. DOI: 10.1007/s00410-017-1416-3.

Mercier, J., D. Sorel, P. Vergely, and K. Simeakis (1989). "Extensional tectonic regimes in the Aegean basins during the Cenozoic". *Basin Research* 2, pages 49–71. DOI: 10.1111/j.1365-2117.1989.tb00026.x.

Michaud, V., R. Clocchiatti, and S. Sbrana (2000). "The Minoan and post-Minoan eruptions, Santorini (Greece), in the light of melt inclusions: chlorine and sulphur behaviour". *Journal of Volcanology and Geothermal Research* 99, pages 195–214. DOI: 10.1016/S0377-0273(00)00173-6.

Mollo, S., P. Del Gaudio, G. Ventura, G. Iezzi, and P. Scarlato (2010). "Dependence of clinopyroxene composition on cooling rate in basaltic magmas: implications for thermobarometry". *Lithos* 118, pages 302–312. DOI: 10.1016/j.lithos.2010.05.006.

Morse, S. (1976). "The lever rule with fractional crystallisation and fusion". *American Journal of Science* 276, pages 330–346. DOI: 10.2475/ajs.276.3.330.

Mortazavi, M. and R. Sparks (2004). "Origin of rhyolite and rhyodacite lavas and associated mafic inclusions of Cape Akrotiri, Santorini: the role of wet basalt in generating calcalkaline silicic magmas". *Contributions to Mineralogy and Petrology* 146, pages 397–413. DOI: 10.1007/s00410-003-0508-4.

Muehlenbachs, K. and G. Byerly (1982). "18O enrichment of silicic magmas caused by crystal fractionation at the Galapagos spreading center". *Contributions to Mineralogy and Petrology* 79, pages 76–79. DOI: 10.1007/BF00376963.

Neave, D. and K. Putirka (2017). "A new clinopyroxene-liquid barometer, and implications for magma storage pressures under Icelandic rift zones". *American Mineralogist* 102, pages 777–794. DOI: 10.2138/am-2017-5968.

Nicholls, I. A. (1971a). "Calcareous inclusions in lavas and agglomerates of Santorini volcano". *Contributions to Mineralogy and Petrology* 30, pages 261–276. DOI: 10.1007/BF00404722.

– (1971b). "Petrology of Santorini volcano, Cyclades, Greece". *Journal of Petrology* 12, pages 67–119. DOI: 10.1093/petrology/12.1.67.

Nomikou, P., C. Hübscher, and S. Carey (2019). "The Christiana–Santorini–Kolumbo Volcanic Field". *Elements* 15, pages 171–176. DOI: 10.2138/gselements.15.3.171.

Palme, H. and H. O'Neill (2014). "Cosmochemical estimates of mantle composition". *Treatise on Geochemistry*. 2nd Edition. Elsevier, pages 1–39. DOI: 10.1016/B978-0-08-095975-7.00201-1.

Panienka, S. (2012). "The Concentration of Lithium in Plagioclase Crystals of the Minoan Tephra (Santorini, Greece)". PhD thesis. Ruprecht-Karls-Universität, Heidelberg. DOI: 10.11588/heidok.00013078.

Pank, K., T. Hansteen, J. Geldmacher, F. Hauff, B. Jicha, P. Nomikou, D. Garbe-Schönberg, and K. Hoernle (2022). "Mineralogy and geochemistry of lavas from the submarine lower caldera walls of Santorini Volcano (Greece)". *Journal of Volcanology and Geothermal Research* 427, page 107556. DOI: 10.1016/j.jvolgeores.2022.107556.

Papazachos, C. (2019). "Deep structure and active tectonics of the South Aegean volcanic arc". *Elements* 15, pages 153–158. DOI: 10.2138/gselements.15.3.153.

Pe-Piper, G., D. Piper, and P. Reynolds (1983). "Paleomagnetic stratigraphy and radiometric dating of the Pliocene volcanic rocks of Aegina, Greece". *Bulletin Volcanologique* 46, pages 1–7. DOI: 10.1007/BF02598241.

Putirka, K. (2008). "Thermometers and barometers for volcanic systems". *Reviews in Mineralogy and Geochemistry* 69, pages 61–120. DOI: 10.2138/rmg.2008.69.3.

Putlitz, B., A. Matthews, and J. Valley (2000). "Oxygen and hydrogen isotope study of high-pressure metagabbros and metabasalts (Cyclades, Greece): implications for the subduction of oceanic crust". *Contributions to Mineralogy and Petrology* 138, pages 114–126. DOI: 10.1007/s004100050012.

Rose, N. and D. Bird (1994). "Hydrothermally altered dolerite dykes in East Greenland: implications for Ca-metasomatism of basaltic protoliths". *Contributions to Mineralogy and Petrology* 116, pages 420–432. DOI: 10.1007/BF00310909.

Santo, A. (2005). "Magmatic evolution processes as recorded in plagioclase phenocrysts of Nea Kameni rocks (Santorini Volcano, Greece)". *Developments in Volcanology*. Elsevier, pages 139–160.

Satow, C., A. Gudmundsson, R. Gertisser, C. Bronk Ramsey, M. Bazargan, D. Pyle, S. Wulf, A. Miles, and M. Hardiman (2021). "Eruptive activity of the Santorini Volcano controlled by sea-level rise and fall". *Nature Geoscience* 14, pages 586–592. DOI: 10.1038/s41561-021-00783-4.

Simmons, J. M., R. J. Carey, R. A. F. Cas, and T. H. Druitt (2017). "High magma decompression rates at the peak of a violent caldera-forming eruption (Lower Pumice 1 eruption, Santorini, Greece)". *Bulletin of Volcanology* 79, page 42. DOI: 10.1007/s00445-017-1120-1.

Sisson, T. and T. Grove (1993). "Experimental investigations of the role of H_2O in calc-alkaline differentiation and subduction zone magmatism". *Contributions to Mineralogy and Petrology* 113, pages 143–166. DOI: 10.1007/BF00283225.

Skarpelis, N. and A. Liati (1990). "The prevolcanic basement of Thera at Athinios: metamorphism, plutonism and mineralization". *Thera and the Aegean World III*. Volume 2, pages 172–182.

Smith, D. (2014). "Clinopyroxene precursors to amphibole sponge in arc crust". *Nature Communications* 5, page 4329. DOI: 10.1038/ncomms5329.

Stamper, C., J. Blundy, R. Arculus, and E. Melekhova (2014). "Petrology of Plutonic Xenoliths and Volcanic Rocks from Grenada, Lesser Antilles". *Journal of Petrology* 55, pages 1353–1387. DOI: 10.1093/petrology/egu027.

Streckeisen, A. (1974). "Classification and nomenclature of plutonic rocks". *Geologische Rundschau* 63, pages 773–786. DOI: 10.1007/BF01820841.

Sun, C., M. Graff, and Y. Liang (2017). "Trace element partitioning between plagioclase and silicate melt: The importance of temperature and plagioclase composition, with implications for terrestrial and lunar magmatism". *Geochimica et Cosmochimica Acta* 206, pages 273–295. DOI: 10.1016/j.gca.2017.03.003.

Sun, C. and Y. Liang (2012). "Distribution of REE between clinopyroxene and basaltic melt along a mantle adiabat: effects of major element composition, water, and temperature". *Contributions to Mineralogy and Petrology* 163, pages 807–823. DOI: 10.1007/s00410-011-0700-x.

Taylor, S. and S. McLennan (1985). *The continental crust: Its composition and evolution*. Oxford: Blackwell Scientific Publications.

Tiepolo, M., A. Langone, T. Morishita, and M. Yuhara (2012). "On the recycling of amphibole-rich ultramafic intrusive rocks in the arc crust: evidence from Shikanoshima Island (Kyushu, Japan)". *Journal of Petrology* 53, pages 1255–1285. DOI: 10.1093/petrology/egs016.

Tollan, P., I. Bindeman, and J. Blundy (2012). "Cumulate xenoliths from St. Vincent, Lesser Antilles Island Arc: a window into upper crustal differentiation of mantle-derived basalts". *Contributions to Mineralogy and Petrology* 163, pages 189–208. DOI: 10.1007/s00410-011-0665-9.

Turner, S., J. Foden, R. George, P. Evans, R. Varne, M. Elburg, and G. Jenner (2003). "Rates and processes of potassic magma evolution beneath Sangeang Api volcano, East Sunda Arc, Indonesia". *Journal of Petrology* 44, pages 491–515. DOI: 10.1093/petrology/44.3.491.

Vaggelli, G., M. Pellegrini, G. Vougioukalakis, S. Innocenti, and L. Francalanci (2009). "Highly Sr radiogenic tholeiitic magmas in the latest inter-Plinian activity of Santorini volcano, Greece". *Journal of Geophysical Research: Solid Earth* 114, B06201. DOI: 10.1029/2008JB005936.

Vakhrameeva, P., A. Koutsodendris, S. Wulf, W. Fletcher, O. Appelt, M. Knipping, R. Gertisser, M. Trieloff, and J. Pross (2018). "The cryptotephra record of the Marine Isotope Stage 12 to 10 interval (460-335 ka) at Tenaghi Philippon, Greece: Exploring chronological markers for the Middle Pleistocene of the Mediterranean region". *Quaternary Science Reviews* 200, pages 313–333. DOI: 10.1016/j.quascirev.2018.09.019.

Van Orman, J., T. Grove, and N. Shimizu (2001). "Rare earth element diffusion in diopside: Influence of temperature, pressure, and ionic radius, and an elastic model for diffusion in silicates". *Contributions to Mineralogy and Petrology* 141, pages 687–703. DOI: 10.1007/s004100100269.

Vespa, M., J. Keller, and R. Gertisser (2006). "Interplinian explosive activity of Santorini volcano (Greece) during the past 150,000 years". *Journal of Volcanology and Geothermal Research* 153, pages 262–286. DOI: 10.1016/j.jvolgeores.2005.12.009.

Vougioukalakis, G. E., C. G. Satow, and T. H. Druitt (2019). "Volcanism of the South Aegean volcanic arc". *Elements* 15, pages 159–164. DOI: 10.2138/gselements.15.3.159.

Whitley, S., R. Halama, R. Gertisser, K. Preece, F. Deegan, and V. Troll (2020). "Magmatic and Metasomatic Effects of Magma–Carbonate Interaction Recorded in Calc-silicate Xenoliths from Merapi Volcano (Indonesia)". *Journal of Petrology* 61, egaa048. DOI: 10.1093/petrology/egaa048.

Wulf, S., J. Keller, C. Satow, R. Gertisser, M. Kraml, K. Grant, O. Appel, P. Vakhrameeva, A. Koutsodendris, M. Hardiman, H. Schulz, and J. Pross (2020). "Advancing Santorini's tephrostratigraphy: New glass geochemical data and improved marine-terrestrial tephra correlations for the past 360 kyrs". *Earth-Science Reviews* 200, page 102964. DOI: 10.1016/j.earscirev.2019.102964.

Wyers, G. (1987). "Petrogenesis of calc-alkaline and alkaline magmas from the southern and eastern Aegean Sea, Greece". PhD thesis. The Ohio State University.

Yanagida, Y., M. Nakamura, A. Yasuda, T. Kuritani, M. Nakagawa, and T. Yoshida (2018). "Differentiation of a hydrous arc magma recorded in melt inclusions in deep crustal cumulate xenoliths from Ichinomegata Maar, NE Japan". *Geochemistry, Geophysics, Geosystems* 19, pages 838–864. DOI: 10.1002/2017GC007301.

Zheng, Y.-F. (1993). "Calculation of oxygen isotope fractionation in anhydrous silicate minerals". *Geochimica et Cosmochimica Acta* 57, pages 1079–1091. DOI: 10.1016/0016-7037(93)90042-U.